

Revista Română de Inginerie Civilă

Indexată în bazele de date internaționale (BDI)

ProQuest, INSPEC, EBSCO, GOOGLE SCHOLAR, CROSSREF, TDNET,
DIMENSIONS, DRJI, JGATE, INDEX COPERNICUS, ULRICH'S și
JOURNALSEEK

Volumul 14 (2023), Numărul 2

- Flow variation and fuel savings when using Hydrogen-Methane mixture as combustible in wall-mounted boilers' operation
Variația debitului și economiile de combustibil la utilizarea amestecului de hidrogen-metan ca combustibil în funcționarea cazanelor montate pe perete 61-72
Răzvan CALOTĂ, Paul-Dan STĂNESCU
-
- Studiu comparativ privind coroziunea în timp a electrozilor în sol, Partea 4 – Predicția matematică și prototip
Comparative study regarding corrosion in time of the ground electrodes, Part 4 – Mathematical prediction and prototype 73-86
Ștefan PAVEL, Ioan Bogdan PASCU, Nicoleta NEMEȘ, Romeo NEGREA, Emilia DOBRIN, Oana BURIAC
-
- Glazed elements in constructions. Evaluation methods of characteristics and their impact on energy performance
Elemente vitrate în construcții. Metode de evaluare a caracteristicilor și impactul acestora asupra performanței energetice 87-95
Simon PESCARI, Alexandru Florin PITROACĂ, Mircea Răzvan MEREĂ, Valeriu-Augustin STOIAN
-
- Influența factorilor de ventilare asupra dezvoltării incendiilor în încăperi și clădiri. Recenzie studii numerice
The influence of ventilation factors on the development of fires in rooms and buildings. Review of numerical studies 96-106
Iulian-Cristian ENE, Vlad IORDACHE, Alexandru-George BECHERU
-
- Optimizarea termodinamica a unui sistem hibrid inovativ care utilizeaza captatoare solare si pompa de caldura pentru date climatice zilnice
Thermodynamic optimization of a novel hybrid system using solar collector and heat pump based on daily weather data 107-119
Florin IORDACHE, Mugurel TALPIGA
-
- Microsilica and steel dust as nano- and micro-particles addition for increasing the mechanical strength of fly ash and blast furnace slag-geopolymer concrete
Microsilica și praf de oțel ca adaos de nano și microparticule pentru creșterea rezistenței mecanice a betonului geopolimeric pe bază de cenușă zburătoare și zgură de furnal 120-129
Bogdan-Valentin PĂUNESCU, Lucian PĂUNESCU, Enikő VOLCEANOV
-
- Aesthetics and Visualization of Building Projects in BIM Environment
Estetica și vizualizarea proiectelor de construcții în mediul BIM 130-145
Marian-Valentin POPESCU, Mădălina STOIAN, Andreea GRECU

MATRIX ROM
3 Politehnicii Street, Bucharest, Romania
Tel. +4021.4113617, +40733882137
e-mail: office@matrixrom.ro
www.matrixrom.ro

EDITORIAL BOARD

Ph.D. Assoc. Prof. Arch. Eur. Ing. Lino BIANCO, *University of Malta, Malta*
Ph.D.Prof.Eng. Ioan BOIAN, *Transilvania University of Brasov, Romania*
Ph.D.Prof.Eng. Ioan BORZA, *Polytechnic University of Timisoara, Romania*
Ph.D.Assoc.Prof.Eng. Vasilică CIOCAN, *Gh. Asachi Technical University of Iași, Romania*
Ph.D.Prof. Stefano CORGNATI, *Politecnico di Torino, Italy*
Ph.D.Assoc.Prof.Eng. Andrei DAMIAN, *Technical University of Constructions Bucharest, Romania*
Ph.D.Prof. Yves FAUTRELLE, *Grenoble Institute of Technology, France*
Ph.D.Prof.Eng. Carlos Infante FERREIRA, *Delft University of Technology, The Netherlands*
Ph.D.Prof. Manuel GAMEIRO da SILVA, *University of Coimbra, Portugal*
Ph.D.Prof.Eng. Dragoș HERA, *Technical University of Constructions Bucharest, Romania, honorary member*
Ph.D. Jaap HOGELING, *Dutch Building Services Knowledge Centre, The Netherlands*
Ph.D.Prof.Eng. Ovidiu IANCULESCU, *Romania, honorary member*
Ph.D.Lawyer Cristina Vasilica ICOCIU, *Polytechnic University of Bucharest, Romania*
Ph.D.Prof.Eng. Anica ILIE, *Technical University of Constructions Bucharest, Romania*
Ph.D.Prof.Eng. Gheorghe Constantin IONESCU, *Oradea University, Romania*
Ph.D.Prof.Eng. Florin IORDACHE, *Technical University of Constructions Bucharest, Romania – director editorial*
Ph.D.Prof.Eng. Vlad IORDACHE, *Technical University of Constructions Bucharest, Romania*
Ph.D.Prof.Eng. Karel KABELE, *Czech Technical University, Prague, Czech Republic*
Ph.D.Prof. Birol KILKIS, *Baskent University, Ankara, Turkey*
Ph.D.habil. Assoc.Prof. Zoltan MAGYAR, *Budapest University of Technology and Economics, Hungary*
Ph.D.Assoc.Prof.Eng. Carmen MĂRZA, *Technical University of Cluj Napoca, Romania*
Ph.D.Prof.Eng. Ioan MOGA, *Technical University of Cluj Napoca, Romania*
Ph.D.Assoc.Prof.Eng. Gilles NOTTON, *Pascal Paoli University of Corsica, France*
Ph.D.Prof.Eng. Daniela PREDA, *Technical University of Constructions Bucharest, Romania*
Ph.D.Prof.Eng. Adrian RETEZAN, *Polytechnic University of Timisoara, Romania*
Ph.D.Prof. Emeritus Aleksandar SEDMAK, *University of Belgrad, Serbia*
Ph.D. Boukarta SOUFIANE, *Institute of Architecture and Urban Planning, BLIDA1, Algeria*
Ph.D.Assoc.Prof.Eng. Daniel STOICA, *Technical University of Constructions Bucharest, Romania*
Ph.D.Prof. Branislav TODOROVIĆ, *Belgrad University, Serbia*
Ph.D.Prof. Marija S. TODOROVIĆ, *Academy of Engineering Sciences of Serbia*
Ph.D.Eng. Ionuț-Ovidiu TOMA, *Gh. Asachi Technical University of Iași, Romania*
Ph.D.Prof.Eng. Ioan TUNS, *Transilvania University of Brasov, Romania*
Ph.D.Assoc.Prof.Eng. Constantin ȚULEANU, *Technical University of Moldova Chisinau, Republic of Moldova*
Ph.D.Assoc.Prof.Eng. Eugen VITAN, *Technical University of Cluj Napoca, Romania*

Romanian Journal of Civil Engineering is founded, published and funded by
publishing house MATRIX ROM
Executive Director: mat. Iancu ILIE

Online edition ISSN 2559-7485
Print edition ISSN 2068-3987; ISSN-L 2068-3987

Flow variation and fuel savings when using Hydrogen-Methane mixture as combustible in wall-mounted boilers' operation

Variația debitului și economiile de combustibil la utilizarea amestecului de hidrogen-metan ca combustibil în funcționarea cazanelor montate pe perete

Răzvan CALOTĂ¹, Paul-Dan STĂNESCU²

^{1,2}Department of Thermodynamic Sciences, Faculty of Building Services, Technical University of Civil Engineering Bucharest,
66 Pache Protopopescu Blvd., 020396 Bucharest, Romania;
E-mail: razvan.calota@yahoo.com; pauldan.stanescu@yahoo.com

DOI: 10.37789/rjce.2023.14.2.1

Abstract: *The article presents a theoretical and experimental analysis that highlights how the employment of a hydrogen- methane mixture influences the variation of the fuel flow for wall-mounted boilers and also aims to evaluate whether fuel economy may be achieved. For a 28 kW condensing boiler, at 50/30 °C water outlet/inlet operating regime and for 2800 h functioning, 431 m³ of methane gas were saved when using a 23% hydrogen-methane combustible. Correspondingly, at 80/60 °C working regime 599.3 m³ of methane economy was achieved. The theoretical increasing of the combustible flow of 23,2% is validated by the value obtained experimentally of 22.84% respectively, when the mixture is utilized.*

Keywords: hydrogen combustible; fuel savings

1. Introduction

In order to meet the decarbonization goals established by the European Union for 2050, hydrogen has been identified as a crucial component [1]. Hydrogen has the potential to drastically lower greenhouse gas emissions in a variety of sectors because it is a clean and renewable energy source. Hydrogen fuel cells can be used to power cars in the transportation industry, eliminating the need for gasoline and diesel. This has the potential to significantly reduce transportation-related emissions, which account for a sizable portion of global carbon emissions.

Hydrogen has other use in the industrial sector. When employed as a feedstock in industrial operations, hydrogen can take the place of fossil fuels and greatly reduce emissions. The EU has set an aim of producing at least 40 GW of hydrogen by 2030 and

at least 240 GW by 2050 in order to meet these objectives [2]. This will require substantial investments in hydrogen generation, storage, and distribution. The EU has established a "hydrogen alliance" and also a "hydrogen strategy for a climate-neutral Europe" to unite significant players in the hydrogen industry and cooperate toward shared objectives [3]. Hydrogen can be used in the energy sector in addition to wind and solar energy to build a more steady and dependable power system. Hydrogen can be utilized as a backup energy source at times when the wind and sun aren't producing as much energy.

The price of manufacture is one obstacle to using hydrogen as a combustible. The majority of hydrogen is currently produced using fossil fuels, which has a significant impact on greenhouse gas emissions. The cost of production is anticipated to go down as renewable hydrogen generation techniques progress. The infrastructure required to support the use of hydrogen presents another difficulty. This covers hydrogen production, distribution, and storage as well as the tools and vehicles required to use it. The EU is attempting to overcome these obstacles by funding research and development into technologies for producing and storing hydrogen as well as by encouraging the creation of hydrogen infrastructure. Overall, hydrogen has a big chance to help us reach our 2050 decarbonization goals. One of the actions that can be taken in order to reduce hydrocarbons in the combustibles is by replacing them with hydrogen in the wall-mounted boilers that are a key component of the household heating. This is done while simultaneously taking into account the necessity of reducing CO₂ emissions, especially from the household heating and hot water producing facilities.

The authors have consistently tested and experimented on combustion equipment powered by gaseous, liquid, or solid fuel within the Centre of the Department of Thermal Sciences part of the Technical University of Civil Engineering Bucharest, Romania, in order to evaluate the combustion efficiency. The fact that the experimental setup has received accreditation from the Romanian National Accreditation Body (RENAR) instills trust in the accuracy of the test results [4]. Many researchers have been interested in the concept the essay addresses up until this point. The investigations that have been done thus far are largely theoretical, and the experimental component is necessary to validate the findings. Articles like [5-15] are valuable in the field, but they generally present numerical modeling or process simulations in specialized software, and in the situation where the data are obtained after conducting experiments, the effects of using the methane-hydrogen mixture on the operation of wall-mounted condensing boilers are not highlighted. Among the most challenging studies involved testing a variety of combustion devices to see how a hydrogen-natural gas mixture affected performance and emissions. This experiment was carried out by Shaffert J. et al. [8]. One of the project's primary findings was that, at 30 vol.% hydrogen admixture, a thermal power reduction of up to 12% compared to the operation with natural gas was observed.

To date, the authors have conducted several studies on the impact of hydrogen-methane mixture, when 10, 20 and 23% of hydrogen is used in the mixture. The article "*CO₂ emissions reduction through increasing H₂ participation in gaseous combustible–Condensing boilers functional response*" published in *Applied Sciences* in 2022 concluded that an increase in combustible flow with 16% is needed in order to maintain the boiler thermal power and to overcome the fact that hydrogen has lower net and gross calorific values when compared to methane. The paper "*The direct effect of enriching the gaseous combustible with 23% Hydrogen in condensing boilers' operation*" published in *Energies* in 2022 emphasizes the reduction of carbon dioxide emissions in the atmosphere when using hydrogen in percentage of 23% in the mixture. The annual reduction in CO₂ emissions for a 28 kW condensing boiler averages 1.22 t; this number was obtained experimentally and agrees with the theoretical assessment.

In addition to the conclusions obtained from previous studies this article investigates the flow variation and fuel savings when using Hydrogen- Methane mixture as combustible in wall-mounted boilers' operation. Considering the fact that the combustible flow increases it is mandatory to assess the net methane savings that can be achieved. Secondly, the research examines the differences between the combustion of pure methane and the combustion of a methane-hydrogen mixture from a thermodynamics perspective.

2. Materials and Methods

The installation of a 28 kW condensing boiler with flattened pipes in a specific circuit for testing wall-mounted boilers, in particular, was part of the experimental research described in this article. The stand has several different kinds of sensors for measuring the flow of gaseous combustibles, the temperature of the water, and water flow. Table 1 shows the kind of sensor, measurement cycle, and accuracy. To ensure proper operation and the accuracy of the data shown, all sensors are calibrated every two years.

All test results are confidently supported by the experimental circuit's Renar accreditation, which additionally ensures credibility.

The Experimental Stand is presented in Figure 1 and its design meets the requirements of the European testing standards [16,17].

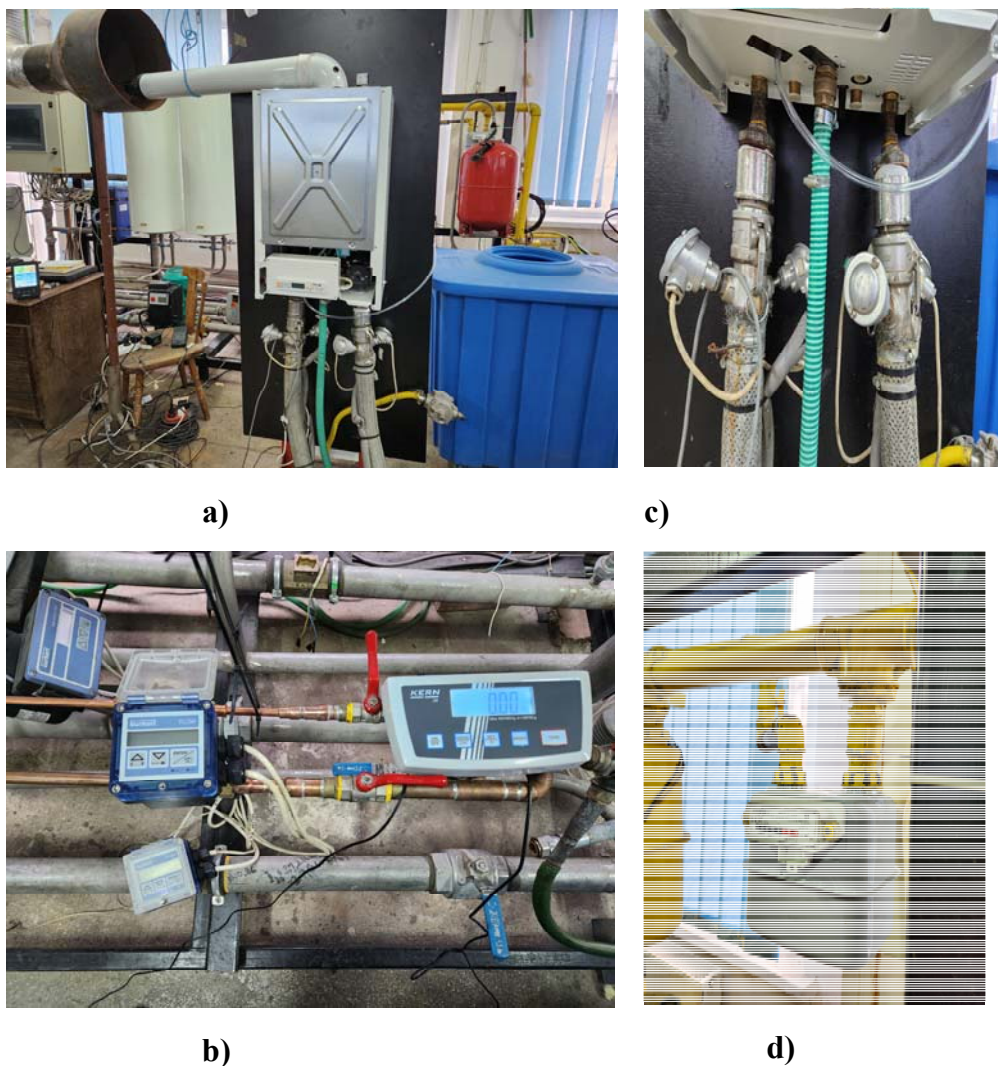


Figure 1. a) Experimental stand b) Water flow meters c) Temperature sensors d) Gas meter (Source: own elaboration)

Table 1.

Measurement sensors (used in this research)

Sensor/ Device	Measurement	Measurement range	Accuracy
Thermal resistance	Temperature $T[^\circ\text{C}]$	-20 to 100 $^\circ\text{C}$	$\pm 0,1\%$
Propeller flow meters	Water velocity [m/s]	0.2 to 10 m/s	$\pm 0,5\%$
Gas meter	Gas flow [m^3/h]	0.6 to 6 m^3/h	$\pm 0,5\%$

Through a theoretical analysis of the combustion process, important parameters necessary for adjusting the experimental stand are determined, such as the theoretical volume of air required for combustion, the theoretical volume of combustion gases and the maximum percentage of CO₂ depending on the type of fuel, which consist an input data for flue gas analyzer setting.

The stoichiometric thermodynamic calculation assumes that combustion takes place without excess air and the chemical reactions are complete. Thermodynamics deals in particular with the phenomena of controlled combustion within thermal equipment and through calculation different parameters can be obtained:

- Determining the volume of air required to burn a fuel with a known chemical composition
- Determination of the excess air required for complete combustion
- Determination of the volume of combustion gases resulting from the combustion process

When combustion results in compounds such as CO, NO, SO, CH₄, it means that the reaction with oxygen of the fuel elements was not complete, or in other words, enough oxygen was not delivered for combustion, resulting in incomplete combustion.

We consider the gaseous fuel unit (one cubic meter) composed of the volume shares "co" of carbon monoxide, "h" of hydrogen, " $c_m h_n$ " of hydrocarbon (each separately), " h_2s " of hydrogen sulfide, "o" of oxygen, " co_2 " of carbon dioxide and "n'" of nitrogen.

Following the analysis of the combustion reaction with oxygen of the combustible components in the gas mixture we can obtain the minimum air volume for gaseous combustible stoichiometric burning (Eq.1), flue gas minimum volume (Eq.2) [18,19].

$$V_{air,min.} = 2,38 \cdot (co + h) + 7,143 \cdot h_2s + 4,762 \cdot \sum \left(m + \frac{n}{4} \right) \cdot c_m h_n \quad (1)$$

$$- 4,762 \cdot o \left[\frac{m^3 air}{m^3 comb.} \right]$$

$$V_{g,min.} = V_{CO_2} + V_{H_2O} + V_{SO_2} + V_{H_2S} + V_{N_2}$$

$$= 0,01 \cdot (co + co_2 + \sum m \cdot c_m h_n) + 0,01 \cdot (h + h_2s + \sum \frac{n}{2} \cdot c_m h_n)$$

$$+ 0,01 \cdot h_2s + (0,01 \cdot n' + 0,79 \cdot V_{aer,min.}) \left[\frac{m^3 gases}{m^3 comb} \right] \quad (2)$$

$$V_g = V_{g,\min.} + (\lambda - 1) \cdot V_{\text{air},\min.} \left[\frac{\text{m}^3 \text{ gases}}{\text{m}^3 \text{ comb.}} \right] \quad (3)$$

The theoretical evaluation involves the consideration of initial values for certain quantities such as excess air, λ and operating efficiency, η . All these values will be estimated based on the experience of testing similar equipment. The excess air can be considered to be 1.3, which consists of an average value for this parameter obtained by the authors during noticeably testing activities. By inserting the excess air into Eq.(3) the total volume of flue gases is obtained.

In order to carry out the study, we used the technical sheets of the gas cylinders used in the experimental part. Two type of gases were used, namely G20 which is essentially methane and G222, a mixture between methane and 23% hydrogen. This specific composition is clearly described in the test standards [20].

The volumetric composition was taken from these sheets.

The percentage volume shares of the components in the mixture are presented in Table 2. The components present as residues in the G20 mixture (isobutane, hydrogen, carbon monoxide, isopentane, etc.) constituted a maximum percentage of 0.1% and were neglected.

Table 2.

Gaseous combustible composition

Combustible type	Volumetric composition
G222	h 23%; $c_m h_n \Rightarrow ch_4$ 77%
G20	$c_m h_n \Rightarrow ch_4$ 95,6% $c_2 h_6$ 3,24%; $c_3 h_8$ 0,54%; $c_4 h_{10}$ 0,08%; co_2 0,44%

Another important parameter regarding the gaseous fuel is the net heat of combustion (lower calorific value). This quantity was also extracted from the data sheets of the two substances, at the reference temperature of 0°C. G222 has a value of 29,930 kJ/m³ and G20 a value of 36,879 kJ/m³ respectively. From the start it can be seen that the mixture of 23% hydrogen with methane produces a lower amount of heat when compared to pure methane.

Combustible flow is related to the lower calorific value, boiler thermal power and its efficiency as in Eq (3).

$$B = \frac{\dot{Q}}{\eta \cdot H_i} \left[\frac{\text{m}^3 \text{ comb.}}{\text{s}} \right] \quad (4)$$

The tested equipment is a wall-mounted condensing boiler, flattened pipe type with a declared nominal heat load of 28 kW.

To be able to theoretically obtain the combustible flow required for operation, for each gaseous fuel, the efficiency was considered 97%, an averaged value for similar equipment based on the testing team's experience.

3. Results

This section contains theoretical and experimental results regarding the combustible flow variation when converting from methane gas (G20) to a 23% hydrogen- methane mixture (G222).

From theoretically point of view the volume of fuel consumed is determined by applying Eq. (4). The results are presented in Table 3.

Table 3.

Gaseous combustible flow (theoretical)

Combustible flow	G222	G20
$B_{\text{comb.}} \left[\frac{\text{m}^3 \text{comb.}}{\text{h}} \right]$	3,472	2,818

Theoretically, the combustible flow should increase with 23,2% when converting to G222 from G20 gas.

By using Eq. (1) and (3), air and total flue gases volume can be determined. The results are plotted in Table 4.

Table 4.

Air and flue gases volume (thermodynamic analysis)

Parameter	G222	G20
$V_{\text{air,min.}} \left[\frac{\text{m}^3 \text{air}}{\text{m}^3 \text{comb.}} \right]$	7.88	9.798
$V_{\text{air}} \left[\frac{\text{m}^3 \text{air}}{\text{m}^3 \text{comb.}} \right]$	10.244	12.737
$V_{\text{g,min.}} \left[\frac{\text{m}^3 \text{gases}}{\text{m}^3 \text{comb.}} \right]$	8.891	10.976
$V_{\text{g}} \left[\frac{\text{m}^3 \text{gases}}{\text{m}^3 \text{comb.}} \right]$	11.255	13.915

In addition to the theoretical results, the outcome of the experimental study are also presented.

A complete test procedure for a wall-mounted boiler, in addition to safety tests, verification of the proper operation of the measurement sensors, determination of the consumed electrical energy, must contain experimental data sets recorded in stationary working regime, for the following situations:

- Nominal, average, reduced thermal load (30% of nominal load) for the working regime represented by the outlet/inlet temperature of the heating agent 80/60 °C
- Nominal, medium and reduced thermal load for the 50/30 °C condensing operating mode
- For NO_x emissions, tests are carried out at partial thermal loads of 20%, 40%, 60% and 70% of the nominal thermal load and then the values are averaged according to the formula in the standard for determining the class of NO_x emissions.

According to the testing Standards [18,19], the experimental research can only be conducted under circumstances where the monitored parameters do not vary for a period of 10 minutes by more than 0,5 °C for working agent temperatures and by more than 0,5% for flow. For this study the testing was conducted only at nominal thermal load of 28 kW for 50/30 °C and 80/60 °C operating regimes.

Only significant parameters for this study were extracted from the experimental data and are presented in Table 5. The values are averaged for a 10 minute testing time interval.

Table 5.

Experimental values

Combusti	Water	Gas flow	Water [°C]	Water [°C]	Excess air	Operating
G222	1194	3.383	49.78	30.3	1.33	50/30 °C
G20	1246	2.754	50.04	29.7	1.31	
G222	1108	3.307	80.04	60.33	1.33	80/60 °C
G20	1130	2.764	80.18	60.3	1.31	

4. Discussion

In the the authors' previous research, emphasis was placed especially on the reduction of carbon dioxide emissions when hydrogen is used in a mixture with methane gas.

Turning the attention only to the combustible flow consumed per hour and taking into account the fact that the G222 mixture contains 23% hydrogen the following aspects should be emphasized:

For the 50/30 °C operating regime, the condensing operating regime, the average G20 flow rate is 2.754 m³/h and the G222 flow rate is 3.383 m³/h. Thus, in percentage terms, an experimental increase in flow rate by 22.84% is found. Considering the G222 mixture, the percentage of methane is 77%, thus the flow consumed in operation, only referring to methane gas, is 2.6 m³/h. Therefore, a total saving of methane gas obtained when switching from G20 to G222 fuel of 0.154 m³/h. If we relate this value to an average operating time of 2800 hours per year, we obtain an economy of 431 m³ of methane gas, which in the future context of overcharging per cubic meter of gas is significant. This value only concerns one plant, but when it is extrapolated to the total number of wall-mounted boilers that could be fed with G222 mixture, the effect can be significant.

For the 80/60 °C working regime, the average flow rate of G20 is 2.764 m³/h and the flow rate of G222 is 3.307 m³/h. Thus, an experimental increase in flow rate by 19.64% is found. For the G222 mixture, the flow consumed in operation, concerning only the methane gas, is 2.55 m³/h. The saving of methane gas obtained when switching from G20 to G222 fuel is 0.214 m³/h. For an yearly operating time of 2800 hours, 599.3 m³ economy of methane gas is achieved. The results obtained for both operating regimes are similar since the fuel flow doesn't have an important variation. However, the results related to the condensing mode of operation 50/30 °C, where the efficiency is the highest are more important and will be further considered as reference.

In view of air and total gas volumes, by analyzing Table 4, an increase of both values can be noticed, when using G222 in comparison with G20. Thus, the total air volume is 19.57% lower and the total flue gases volume is 19,11% lower relative to a cubic meter of combustible. However, this values can be misleading if the fact that the flow is higher when dealing with G222 (Table 3) due to its lower calorific value. In line with this aspect, the air flow and flue gases flow are determined and presented in Table 6.

Table 6.

Air and flue gases flow (thermodynamic analysis)

Parameter	G222	G20
$\dot{V}_{\text{air}} \left[\frac{\text{m}^3 \text{air}}{\text{h}} \right]$	35.57	35.89
$\dot{V}_{\text{g}} \left[\frac{\text{m}^3 \text{gases}}{\text{h}} \right]$	39.08	39.21

Furthermore, from the experimental data plotted in Table 5, the excess air is slightly higher when the boiler is fed with G222, so in both cases the air volume and the flue gases volume are roughly similar.

When comparing the experimental data with the theoretical ones, it can be seen that the initially assumed value for the excess air is confirmed and also the difference between the fuel flow values in the two analyzed cases is validated. The theoretical value of 23,2% is validated by the value obtained experimentally of 22.84% respectively.

5. Conclusions

When methane is released into the atmosphere, it acts as a potent greenhouse gas and accelerates climate change. The only result of hydrogen combustion, on the other hand, is water vapor, making it a cleaner and greener alternative. Additionally, some industrial processes can be made more cost-effective and efficient by employing hydrogen as a fuel source in boilers. It is important, however, that in the case of the hydrogen implementation of as a fuel, there should be deductions at the level of European Union like in the case of Germany. This research focuses on the combustible flow variation, when converting from G20 (methane gas) to G222 (23% hydrogen and 77% methane) in wall-mounted boilers' operation. A roughly 23% flow increase was discovered both theoretically and experimentally. With regard to methane savings, in condensing operating regime, only one plant can achieve 431 cubic meters savings yearly. The authors will continue the experimental research with fuel mixtures containing higher percentages of hydrogen to investigate both the behavior from the point of view of the energy efficiency, greenhouse gas emissions and the safety in operation at the burner level.

References

1. https://climate.ec.europa.eu/eu-action/climate-strategies-targets/2050-long-term-strategy_en (accessed on 15 December 2022).
2. https://energy.ec.europa.eu/topics/energy-systems-integration/hydrogen_en (accessed on 15 December 2022).
3. <https://eur-lex.europa.eu/legal-content/EN/TXT/?uri=CELEX:52020DC0301> (accessed on 19 December 2022).
4. https://www.renar.ro/index.php/oec/get_oec_details/41741 (accessed on 20 December 2022).
5. Yue Xin, Ke Wang, Yindi Zhang, Fanjin Zeng, Xiang He, Shadrack Adjei Takyi and Paitoon Tontiwachwuthikul Numerical Simulation of Combustion of Natural Gas Mixed with Hydrogen in Gas Boilers, *Energies* 2021, 14, 6883; <https://doi.org/10.3390/en14216883>

6. Jörg Leicher, Johannes Schaffert, Hristina Cigarida, Eren Tali, Frank Burmeister, Anne Giese, Rolf Albus, Klaus Görner, Stéphane Carpentier, Patrick Milin and Jean Schweitzer- The Impact of Hydrogen Admixture into Natural Gas on Residential and Commercial Gas Appliances, *Energies* **2022**, 15, 777. <https://doi.org/10.3390/en15030777>
7. Paul Glanville, Alex Fridlyand, Brian Sutherland, Mirosław Liszka, Yan Zhao, Luke Bingham and Kris Jorgensen- Impact of Hydrogen/Natural Gas Blends on Partially Premixed Combustion Equipment: NOx Emission and Operational Performance, *Energies* **2022**, 15, 1706. <https://doi.org/10.3390/en15051706>
8. Schaffert, J.; Fischer, P.; Leicher, J.; Burmeister, F.; Flayyih, M.; Cigarida, H.; Albus, R.; Görner, K.; Mili, P.; Carpentier, S.; et al. Impact of Hydrogen Admixture on Combustion Processes—Part II: Practice. Deliverable D2.3 as Submitted from the THyGA Project. 2020. Available online: https://thyga-project.eu/wp-content/uploads/20201211-D2.3-Impact-of-Hydrogen-in-Practice_final.pdf (accessed on 03 March 2022).
9. Suchovsky, C.J., Ericksen, L., Williams, T.A., Nikolic, D.J. (2021). Appliance and Equipment Performance with Hydrogen-Enriched Natural Gases. Canadian Standards Association, Toronto, ON.
10. Harmen de Vriese,, Howard B. Levinskyb- Flashback, burning velocities and hydrogen admixture: Domestic applianceapproval, gas regulation and appliance development, *Applied Energy* **259** (2020) 114116, <https://doi.org/10.1016/j.apenergy.2019.114116>
11. M.S.Boulahlib, F.Medaerts, M.A.Boukhalfac, Experimental study of a domestic boiler using hydrogen methane blend and fuel-rich staged combustion, *International Journal of Hydrogen Energy*, Volume 46, Issue 75, 29 October 2021, Pages 37628-37640, <https://doi.org/10.1016/j.ijhydene.2021.01.103>
12. Gianluigi Lo Basso, Benedetto Nastasi, Davide Astiaso, Garcia Fabrizio Cumo, How to handle the Hydrogen enriched Natural Gas blends I combustion efficiency measurement procedure of conventional and condensing boilers, *Energy* **123** (2017) 615e636, <https://dx.doi.org/10.1016/j.energy.2017.02.042>
13. Ruggero Amaduzzi, Marco Ferrarotti and Alessandro Parente- Strategies for Hydrogen-Enriched Methane Flameless Combustion in a Quasi-Industrial Furnace, 2021, *Frontiers in Energy Research*, doi: 10.3389/fenrg.2020.590300
14. Francesco Scignoli , Filippo Vecchio, Francesco Legrottaglie, Enrico Mattarelli and Carlo Alberto Rinaldini- Numerical Investigation of Dual Fuel Combustion on a Compression Ignition Engine Fueled with Hydrogen/Natural Gas Blends, *Fuels* **2022**, 3, 132–151. <https://doi.org/10.3390/fuels3010009>
15. John G. Ingersoll- The Renewable Hydrogen–Methane (RHYME) Transportation Fuel: A Practical First Step in the Realization of the Hydrogen Economy, *Hydrogen* **2022**, 3, 84–112. <https://doi.org/10.3390/hydrogen3010008>
16. EN 15502-2-1:2012+A1:2016, Gas-fired central heating boilers Specific standard for type C appliances and type B2, B3 and B5 appliances of a nominal heat input not exceeding 1 000 kW, <https://magazin.asro.ro/ro/standard/252192> (accessed on 20 December 2022).

17. EN 15502-1:2021, Gas-fired heating boilers - Part 1: General requirements and tests, <https://magazin.asro.ro/ro/standard/277890> (accessed on 20 December 2022).
18. Razvan Calota “Bazele termodinamicii tehnice pentru pompieri”, MATRIX rom Publishing House, 2019, ISBN 978-606-25-0519-6.
19. Antonescu N. Burning installations and boilers with high energetical efficiency and low pollution emissions -2018, 274 pgs. MatrixRom Bucharest – ISBN 978-973-755-699-8
20. EN 437:2021 Test gases. Test pressures. Appliance categories. <https://magazin.asro.ro/ro/standard/276144> (accessed on 11 October 2022)

Studiu comparativ privind coroziunea în timp a electrozilor în sol, Partea 4 – Predicția matematică și prototip

Comparative study regarding corrosion in time of the ground electrodes, Part 4 – Mathematical prediction and prototype

Ștefan PAVEL⁽¹⁾, Ioan Bogdan PASCU⁽²⁾, Nicoleta NEMEȘ⁽²⁾, Romeo NEGREA⁽³⁾, Emilia DOBRIN⁽⁴⁾, Oana BURIAC⁽²⁾

⁽¹⁾Universitatea Politehnica Timișoara-ICER, Romania

Timișoara, str. G.Musicescu, nr. 138

e-mail: pavelstefanel@gmail.com

⁽²⁾Universitatea Politehnica Timișoara-ICER; Romania

e-mail: i.bogdan.pascu93@gmail.com; nicoleta.nemes@upt.ro; oana.grad@upt.ro

⁽³⁾Universitatea Politehnica Timișoara-Departamentul de Matematică, Romania

Timișoara, P-ța Victoriei, nr. 2

e-mail: romeo.negrea@upt.ro

⁽⁴⁾Institutul Național de Cercetare-Dezvoltare în Sudură și Încercări de Materiale Timișoara, Romania

Timișoara, B-dul Mihai Viteazul, nr. 30.

e-mail: emi_dobrin@yahoo.com

DOI: 10.37789/rjce.2023.14.2.2

Rezumat: Obiectivul lucrării este de a prezenta, aspecte referitoare la: coroziunea metalelor acoperite și neacoperite cu zinc în solul orașului Timișoara (electrozi de împământare a Instalației de Legare la Pământ aferentă Instalațiilor Electrice din Construcții), analiza parametrilor de sol, prototipuri de electrozi, măsurători electrice, microbiologice și analiza de prognoză-predicție matematică, materiale și dicționare de termeni aferenți. Un alt aspect prezentat în acest material este efectuarea de măsurători ale spectrului câmpului electromagnetic oscilografiat al elementelor de metal acoperite și neacoperite cu zinc din sol.

Cuvinte cheie: coroziune, electrod de împământare, sol, legare la pământ, microbiologia solului

Abstract: The objective of this paper is to present aspects related to: corrosion of metals covered, and not covered with zinc in the soil of Timișoara (grounding electrodes of a grounding installation related to Electrical Installations of Constructions), analysis of soil parameters, prototype electrodes, electrical, microbiological analysis and mathematical prognosis analysis-prediction, materials, and dictionaries of related terms. Another aspect presented in this material are the measurements related to the spectrum of the oscillograph electromagnetic field of the grounding electrodes, which are covered, and not covered with zinc.

Key words: corrosion, ground electrode, soil, grounding, soil microbiology

1. Mathematical prediction

Dictionary of terms:

Holt-Winters Method [1, 2] Exponential smoothing methods. Smoothing techniques are used to generate smoothed values (attenuation of random fluctuations in the data from which the random component was removed) and to obtain predictions. The simple moving average method assigns equal weights ($1/k$) to all k points. But recent observations provide more relevant information than past observations. So a weighting scheme that assigns decreasing weights to more distant observations would be useful. Exponential smoothing methods assign higher weights to recent observations and they decrease exponentially as they become more distant. These methods are effective when the parameters describing the time series slowly change over time.

Covariance [3, 2] In probability theory and statistics, covariance is the measure of the common variation of two random variables [4]. If the high values of one variable generally correspond to the high values of the other variable, and if the same is true for the small values (i.e. the two variables have similar behaviors), the covariance is positive [5]. On the other hand, if the high values of one variable generally correspond to the low values of the other variable (i.e. the two variables have opposite behaviors), the covariance is negative. Therefore, the covariance sign shows the direction of the linear relationship between the two variables. The magnitude of the covariance is not easy to interpret because it is not normalized and therefore depends on the magnitude of the variables. However, the normalized version of covariance, the correlation coefficient, can show by magnitude the power of the linear relationship.

Correlation [6, 2] In statistics, dependency is a statistical relationship between two random variables or two sets of data. The correlation refers to a wide class of statistical relationships involving dependence. Familiar examples of dependent phenomena include correlations between the physical stature of parents and their children, as well as correlations between the demand curve of a product and its price. For the study of the dependence between two variables, each of them being subjected to a random scattering, methods of correlation analysis are applied. The correlation analysis studies the average law of behavior of each of the variables according to the values of the other variable, as well as the measure of the dependence between the considered variables. Attaching to each value of one of the variables, for example of x by which the independent variable is denoted, the average of the corresponding values of the other variable, denoted y , we obtain pairs of values (x, y) , which in a graphical representation in Cartesian coordinates appear in the form of a multitude of dots. This graphical representation is called the scatter plot (en plot). The correlation / dispersion diagram graphically illustrates pairs of numerical data, with one variable on each axis, observed within a common phenomenon, in order to identify the links (relationships) that are established between them [4]. If the variables are in correlation, the points will follow a line or a curve. The correlation diagram is one of the seven classic tools of quality management.

Predictive analysis [2, 7]. Predictive analysis includes a variety of statistical techniques from data extraction, predictive modeling and machine learning, which analyze current and historical facts to make predictions about future or otherwise unknown events.

Voltage prediction at sample no. 1, because the data are few, the only prediction that can be made is by trend, using the Holt-Winters method (exponential smoothing). So the series of observations:

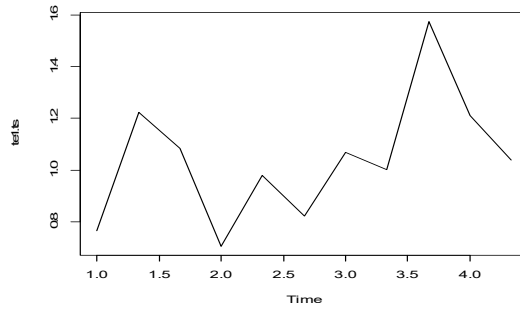


Fig. 1 The series of observations, on the components of the time series

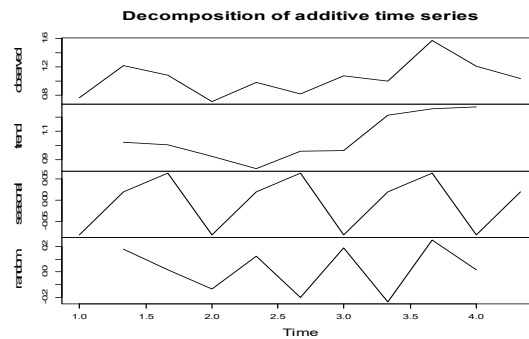


Fig. 2 Holt-Winters analysis (the first graph of the four is the trend)

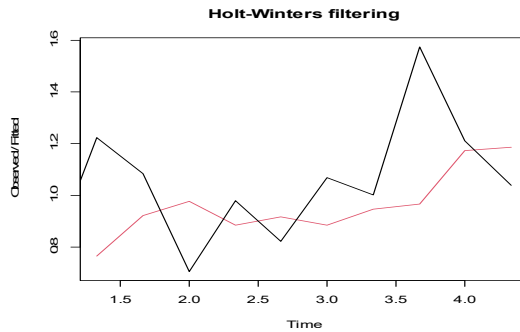


Fig. 3 Holt-Winters analysis (the first graph of the four is the trend)

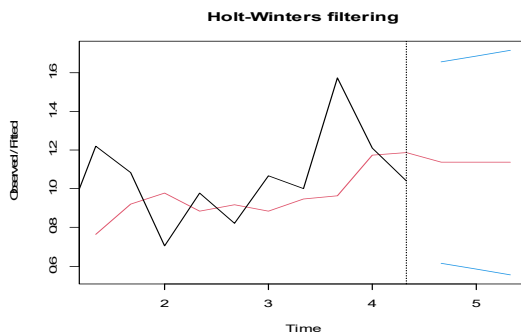


Fig. 4 Holt-Winters prediction (with limits)

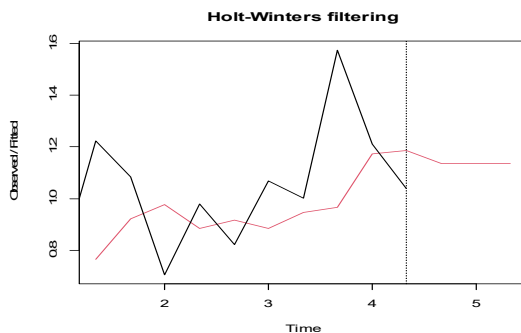


Fig. 5 Holt-Winters prediction (without max and min limits)

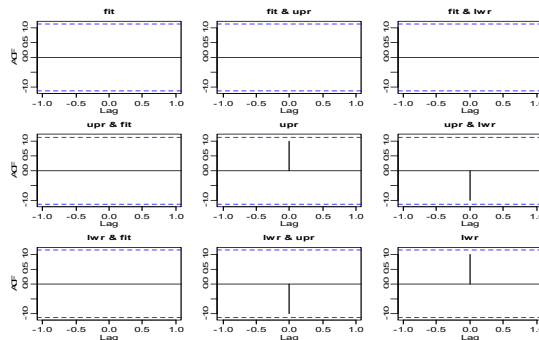


Fig. 6 Study of errors by spectral analysis (autocovariance spectrum)

Prediction for the electrical potential of the sample electrode nr. 1

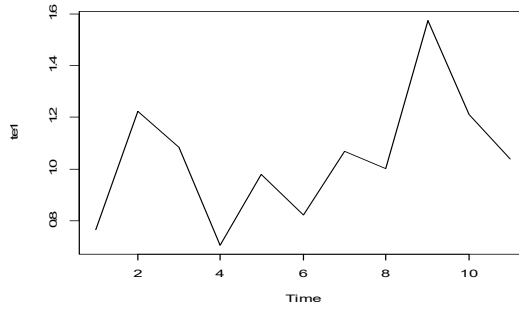


Fig. 7 The series of observations

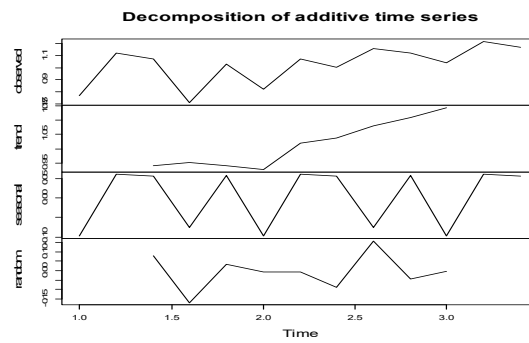


Fig. 8

Series decomposition, first graph = observed series, second graph=trend, third graph = seasonality, fourth graph = random errors

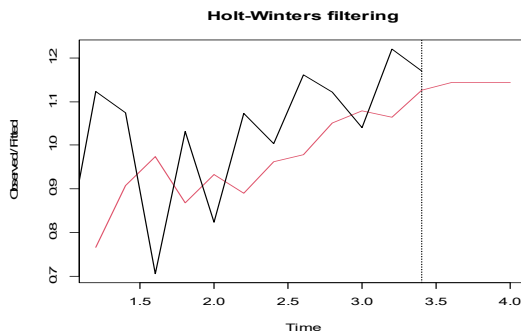


Fig. 9 Tension and prediction by the Holt-Winters method

Correlation meta-analysis (meta-analysis is an analysis of several studies, in our case on several samples-electrodes)

1.1. *Correlation* between tension and current

Five electrode samples were analyzed marked “e1”, “e2”, “e3”, “e4”, “e6” (electrode e5 was excluded because we do not have data on conductivity). 11 data were analyzed (at voltage there were 12 but at current 11, we eliminated the first value from voltage). Graphically we have the following:

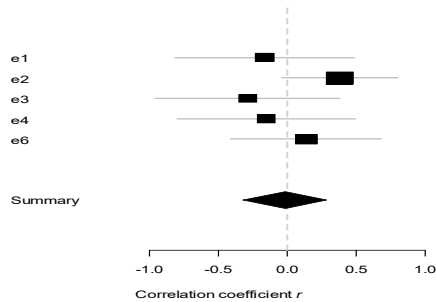


Fig. 10 It can be seen that at: e1, e3, e4 the correlation is slightly negative while at e2 and e6 is slightly positive. These values are the result of a random effect, the fixed effect being close to zero.

In conclusion there is a weak correlation (connection) voltage and current, with different effects. For predictive purposes, it is recommended to analyze voltage and current separately. It can be seen that the electrodes e1, e3 and e4 can be analyzed jointly and analogously for e2 and e6.

1.2. *Correlations between voltage and conductivity*

Graphically we have the following:

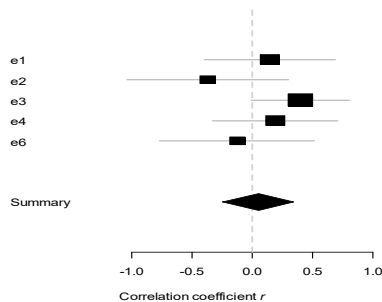


Fig. 11 A positive correlation is observed at: e1, e3 and e4, and at the other two the correlation is negative. The effect is random, the fixed effect being slightly positive. There is not a great correlation between voltage and conductivity, at least the linear connection is not supported from a statistical point of view. It is observed that the electrodes e1, e3 and e4 can be analyzed unitarily and analogously e2 and 26.

1.3. Correlations between current and conductivity

Graphically we have the following:

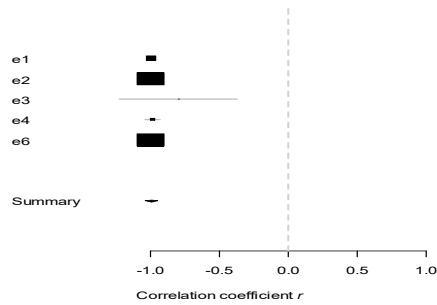


Fig. 12

It is observed that at all 5 electrodes the correlation is about the same, negative close to -1, so an inverse relationship between current and conductivity. In conclusion, the inverse linear connection is statistically supported for all 5 electrodes, as such it is sufficient to make a predictive at the current level and the conductivity is obtained immediately by an inverse linear relationship, $co = a + b *$ with, $b < 0$. It is sufficient to perform the analysis at a single electrode (e2).

1.4. Correlations between resistance and resistivity

The electrode resistance appears in relation to the ground resistivity for the 6 electrodes, having only 4 measured values.

Graphically we have the following:

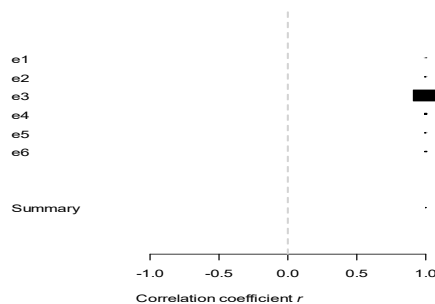


Fig. 13

There is a positive relationship at all 6 electrodes close to 1, so a direct relationship between the 2 quantities. If the e5 electrode is removed from the analysis, we have (similar relationship)

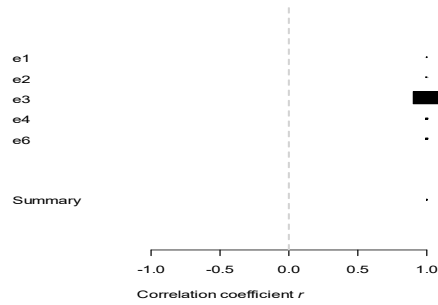


Fig. 14

If the electrode e5 is removed from the analysis, we have (similar relationship). In conclusion, it is enough to know only one quantity, the other is obtained immediately by a direct linear relation of the type $r_{ev} = a + b * r_{ez}$, $b > 0$. It is sufficient to make the prediction at a single electrode (preferably e3).

In conclusion, a predictive of voltage and current on e1 (or e3, or e5) and separated on e2 (or e6) is recommended. Conductivity can be obtained from current prediction. Also, a resistance predictor can be made on only one electrode, or it can be obtained directly if the resistivity is known.

Discussions and conclusions

2. Prototypes

Prototype for remote monitoring of soil corrosion of zinc coated and non - zinc coated metal elements [28]

The technical problem that the prototype solves consists in the realization of an installation for real-time remote monitoring of the corrosion in the ground of the metallic elements covered and not covered with zinc at predetermined depths and the recording, transmission and archiving of the obtained data. The installation for remote monitoring of corrosion in soil of metal elements covered and not covered with zinc according to the prototype consists of a set of metal tubes covered with zinc (of predetermined thicknesses) and not covered with zinc, alternately positioned vertically in the ground at depths predetermined, provided at a certain distance, in parallel, with PVC tubes equipped with elements with electrical conductivity and sensors for measuring temperature and humidity both in the ground and above ground. The entire assembly is connected to a distribution box and a power source powers the control of a remote relay, a microcontroller and a server connected to the internet. The electrical connections downstream of: air and ground temperature and humidity sensors, zinc-coated and non-zinc-coated metal tubes and PVC tubes with electrically conductive elements are connected to the distribution box which is in turn connected to a microcontroller with

HDMI port for a monitor and USB for storing data in CSV format. The microcontroller automatically runs a program designed to record values from elements with electrical conductivity, humidity, and temperature at regular intervals of one second, values that can be viewed on the monitor and stored on the CSV data storage device for processing and analyzed. At the same time, the data recorded from the microcontroller are transmitted to a server where they are processed and stored in a database, "noSQL". The communication with the database is done through a Rest Api interface that also offers a graphical interface accessible to an internet address. The microcontroller and server are connected to the router.

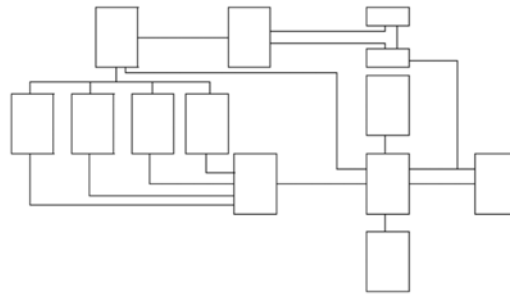


Fig. 15 Schematic diagram of the installation prototype

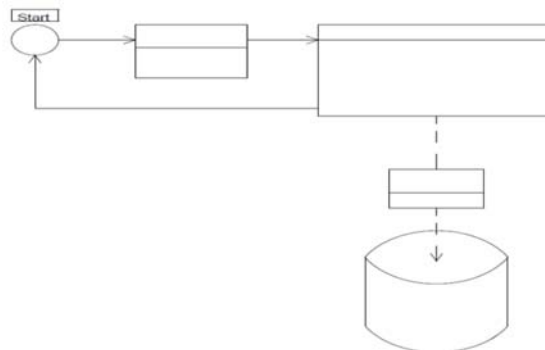


Fig. 16 Schematic of the installation prototype software

BUILDING EARTH ELECTRODE WITH CORROSION RESISTANT CONNECTIONS [9]

The prototype refers to a grounding electrode provided with an anti-corrosion device at the horizontal connection used for the human protection installation against accidental contact voltages in the electrical protection installation of constructions against the effects of lightning. The construction ground electrode with corrosion-resistant connections according to the prototype is connected by welded connections to the (flat strip) of the horizontal part of the construction ground installation. The electrode consists of concentric tubes, an outer galvanized steel tube and an inner galvanized steel

tube joined at the bottom by welding with a flat strip, and at the top by a flat strip with elongated wings and configured in an "S" shape. , so that through the ends of the flat strip to make the connections by welding with the flat strip of the horizontal earthing installation. The connections are coated with bitumen inside corrosion-resistant plastic containers and the upper part of the electrode assembly thus made, respectively the area of the connections between the electrode plate and the horizontal grounding plate is arranged in a visiting room with access for periodic checks and measurements. The outer galvanized steel tube provides at the bottom, on a limited length, at least 4 equidistant longitudinal notches to allow the reflection of the tube material so that on the said tube materialize, transversely on its axis some wings, in the form of a rosette, which defines a larger contact surface of the galvanized steel tube with the ground. The grounding electrode of constructions with corrosion-resistant connections has the following advantages:

- allows better contact with the ground;
- ensures, through a lower electrical resistance, a better passage and dissipation of the lightning overvoltage through the ground;
- ensures the corrosion protection at the joint parts for the flat strip of the horizontal earthing installation;
- ensures a simpler assembly work so that the possibility of friction with the ground is eliminated, implicitly the loss of a zinc microlayer that covers the electrode.

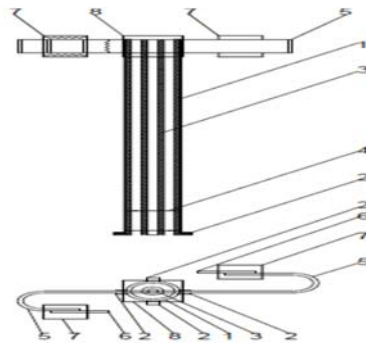


Fig. 17 General diagram of the earth electrode with low electrical resistance and anti-corrosion device

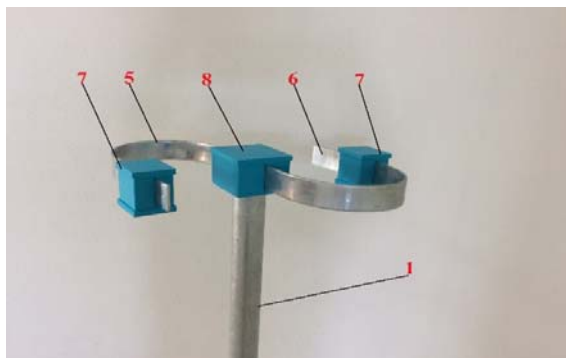


Fig. 18 Imagine foto cu electrodul destinat ILP, prevăzut cu dispozitiv anticoroziune la conexiune;



Fig. 19

Corrosion at the joint area with, weld bead (unprotected) between the vertical and horizontal electrode intended for ILP



Fig. 20

Corrosion-resistant joints with nut (bolt with nut) on the flat band (40X4) of O1 Zn unprotected anticorrosive, intended for ILP



Fig. 21

Corrosion trace joints (contact piece between electrode and round OL Zn profile) for ILP)

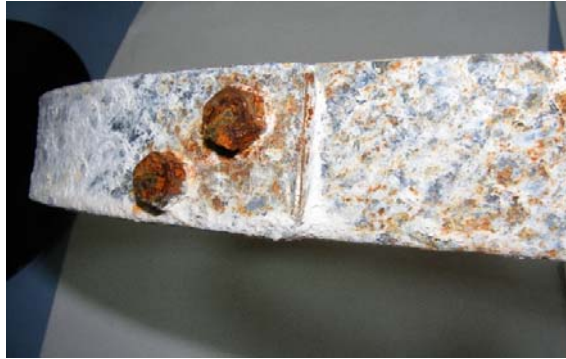


Fig. 22

Joints with corrosion marks (nut screw) on the OL Zn flat strip for ILP



Fig. 23

Bitumen container in the connection area of the horizontal electrode (OL Zn flat strip) for ILP



Fig. 24

Bitumen container in the connection area of the horizontal electrode (OL Zn flat strip) for ILP

It should be mentioned that this type of electrode intended for Grounding Installations, is mounted in the ground in a vertical position after the horizontal trench has been made at the predetermined depth of the norm (the trench is intended for galvanized flat strip of length according to a calculation of ILP - Installation Grounding) the next step being to make penetrations in the ground with the drill (hydraulically or mechanically actuated) at the preset depth of the electrode. The number of electrodes intended for ILP must correspond to that mentioned in the calculation of the ILP related to the dispersion resistance of the earthing.

Example:

Table 1

Calculation example for a grounding installation	
Number of electrodes OL Zn, L=1.5m	15 buc.
Strip OL Zn, 40X4mm cu L=45m	1 buc.
Soil electrical resistivity (clay)	80 Ωm
Dispersion resistance	0.97Ω
Calculation formula	$R = 0.366 \frac{\rho}{l} \lg \frac{4l}{a}$

References

- [1] <https://www.coursehero.com/file/31277167/curs-3-serii-de-timpppt/>
- [2] Romeo Negrea, Modelare statistica și stochastică. Aplicații în inginerie și în economie, Ed. Politehnica, Timișoara, 2006, ISSN (10) 973-625-369-4
- [3] <https://ro.wikipedia.org/wiki/Covarian%C8%9B%C4%83>
- [4] https://ro.wikipedia.org/wiki/Covarian%C8%9B%C4%83#cite_note-1
- [5] https://ro.wikipedia.org/wiki/Covarian%C8%9B%C4%83#cite_note-2
- [6] <https://ro.wikipedia.org/wiki/Corela%C8%9Bie>
- [7] https://en.wikipedia.org/wiki/Predictive_analytics
- [8] Nr. înregistrare O.S.I.M. U/00037 din 03.08.2020
- [9] Nr. înregistrare O.S.I.M. A/ 00757/28.09.2018

Glazed elements in constructions. Evaluation methods of characteristics and their impact on energy performance

Elemente vitrate în construcții. Metode de evaluare a caracteristicilor și impactul acestora asupra performanței energetice

Simon PESCARI¹, Alexandru Florin PITROACĂ¹, Mircea Răzvan MEREA¹, Valeriu-Augustin STOIAN¹

¹Department of Civil Engineering and Building Services Engineering, Faculty of Construction, Polytechnic University of Timișoara

Piața Victoriei, Nr. 2, 300006, Timișoara, Romania

Simon.pescari@upt.ro, alexandru.pitroaca@upt.ro, mircea.merea@student.upt.ro, valeriu.stoian@upt.ro

DOI: 10.37789/rjce.2023.14.2.3

Abstract. *In Glazed elements play an important role in total energy consumption of buildings. They significantly influence total energy consumption through energy consumption for heating and cooling, ventilation and lighting. To optimize these consumptions, the glazed elements must be treated taking into consideration several characteristics, namely: thermal transmittance, degree of transparency and solar factor. Moreover, the choice of glazed elements must be studied and calibrated by the type of building but also by location, from a climatic point of view. The purpose of this paper is to highlight the main characteristics of glazed elements and the ways in which these can be measured. The equipment and its operation are presented as well as examples of measurements performed on different types of glazed elements. Also, the paper presents a case study that includes the thermal balance performed on a building in Timisoara taking into account the characteristics of the measured glazed elements. In order to highlight their importance, a parametric study of the transmittance and the solar factor was performed, taking into account the investment costs, respectively, the cost over the life of the investment.*

Key words: *U-value, g-value, low-e, glazed elements*

1. Introducere

Reducing energy consumption and increasing the energy performance of buildings are two of the most important issues that need to be considered today, whether we are talking about the headquarters of large companies, state institutions or housing, either individually or collectively [1]. The thermal rehabilitation of the building involves improving the thermotechnical characteristics of the envelope elements by adding new layers (in the case of walls, floors when we add a layer of

thermal insulation) or by replacing these elements with more energy efficient ones (in the case of windows, doors).

Glazed elements require more attention when discussing their energy performance [2]. In the design phase of a building, energy consumption can be optimized by correlating the dimensions and properties of glazed elements with the supply of natural light [3,4]. For existing buildings, it can be established by calculation, the replacement of glazed elements with others that can benefit from the available natural light, thus reducing energy consumption.

2. Description of the essential characteristics of glazed elements in terms of energy efficiency

Thermal transmittance of glazing

Thermal transmittance or heat transfer coefficient (U) is the steady-state heat flux, relative to the surface area and the temperature difference between the average temperatures on either side of a system [5]. This is the inverse of thermal resistance. In the case of glazed elements, this is denoted U_g .

Solar heat gain coefficient

Solar heat gain coefficient (g) measures as a percentage the total energy efficiency of the glazed system compared to solar radiation. This is the amount of heat allowed by the sun to pass through the glazed elements [6]. This factor is found directly in the calculation of the heat input of the solar radiation Q_s .

Solar spectrum

In order to better understand the measurements in this paper, the different energy spectra produced by the sun will be explained below. These are the energy spectra that a building is subjected to every day. Some features are positive and we want to benefit from them as much as possible, some are undesirable and should be reduced as much as possible, and others should be kept in a certain balance.

SOLAR SPECTRUM

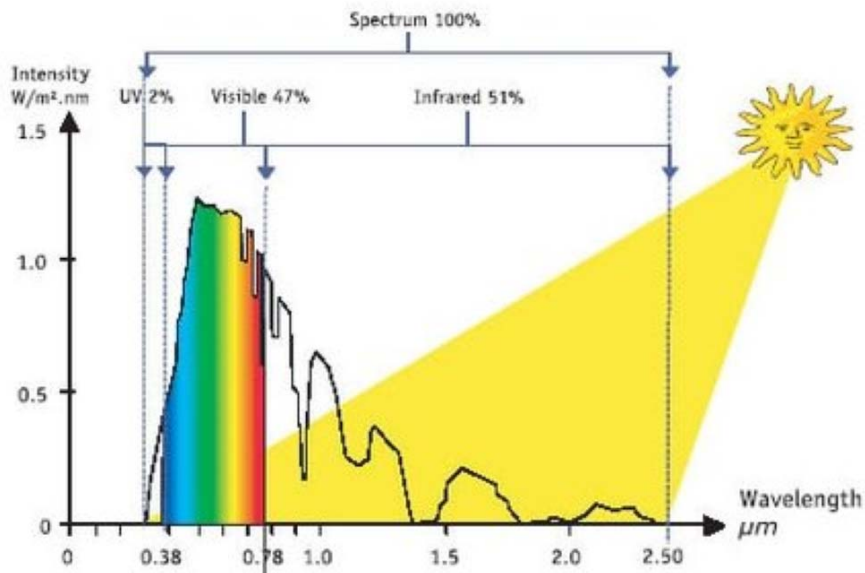


Fig.1. Solar spectrum

Ultraviolet energy is represented by UV rays with wavelength dimensions of 365 nm. This energy is not visible to the human eye and is divided into 3 categories: UVA, UVB, UVC.

Visible light is the only part of the solar spectrum that the human eye can see. This includes the natural light of day and all the colors of the rainbow. A sufficient amount of natural light will reduce the need to use artificial light, thus reducing the cost of utilities.

Infrared energy refers to the thermal energy that is emitted by the sun. It can also be called radiant heat. This is the light that the human eye cannot see, but the bodies feel it as heat. Infrared energy is divided into 2 types: shortwave infrared energy (NIR) and longwave infrared energy (FIR).

The property of a glazed element to repel infrared energy will be directly related to solar heat gain coefficient [6].

3. Case study

In order to be able to carry out the case study, it was proposed to perform measurements to identify the real parameters of the glazed elements.

It is proposed to conduct a case study on a residential building. The study involves calculating the energy required for heating and cooling using, in turn, the types of glazed elements for which the characteristics have been obtained are presented below. The analyzed building is a collective residential building located in the municipality of Timișoara, having a height regime S+P+4E. It was built in 1985,

the resistance structure being made of reinforced concrete structural walls. The building is moderately sheltered and has more than one exposed façade.

The calculation of the energy required for heating and cooling was performed using the non-stationary calculation method. This calculation was performed using the energy simulation program „EnergyPlus”. For all the models, all the characteristics of the building, except those of the glazed elements, remained the same.

The simulations involved calculating the energy required for heating and cooling using, in turn for the entire building, the following types of glazing elements:

- a single glass panel;
- two glass panels;
- two glass panels with a selective layer;
- three glass panels with two selective layers;

As the types of windows improve, so does the permeability of the building. Thus, the number of outdoor air exchanges varies from 0.9 corresponding to a high permeability (case 1-window with 1 glass panel) and decreases to 0.5 corresponding to a low permeability (4 case -window with 3 glass panels with 2 selective layers), according to ISO 13790.

The data entered as well as the energy requirements obtained are presented in the following table:

Table 1

Glazed element type and energy demand

Glazed element type	U_g [W/m²K]	U_f [W/m²K]	U_w [W/m²K]	g	na [h⁻¹]	Heating energy demand [kWh/m²]	Cooling energy demand [kWh/m²]
1 glass panel	5.7	1	4.8	0.86	0.9	135.85	15.2
2 glass panels	2.90	1.00	2.60	0.78	0.7	116.24	14.89
2 glass panels with 1 selective layer	1.10	1.00	1.10	0.38	0.6	110.28	9.45
3 glass panels with 2 selective layers	0.50	1.00	0.76	0.40	0.5	101.39	9.97

To have a better point of view for the obtained data, the energy demand is represented in the next graph:

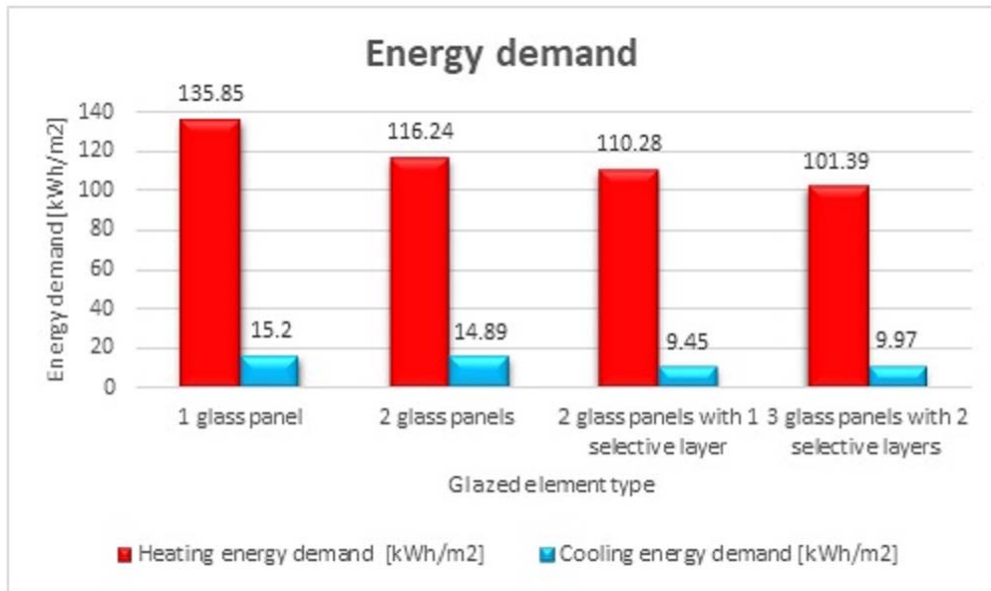


Fig.2. Energy demand graph

Double glazed windows (case 1, $U_g = 2.7 \text{ W/m}^2\text{K}$) reduce the energy required for heating by about 15 % and double glazed windows with a selective coating (case 2, $U_g = 1.1 \text{ W/m}^2\text{K}$) bring a reduction of about 19 % compared to the initial situation. The heat requirement in the case of triple glazing (case 3, $U_g = 0.5 \text{ W/m}^2\text{K}$) decreases by about 25 % compared to the initial situation. Thus, the importance of the solar heat gain coefficient in the heat demand is highlighted, but also the importance of reducing the air infiltrations through the leaks of the glazed elements.

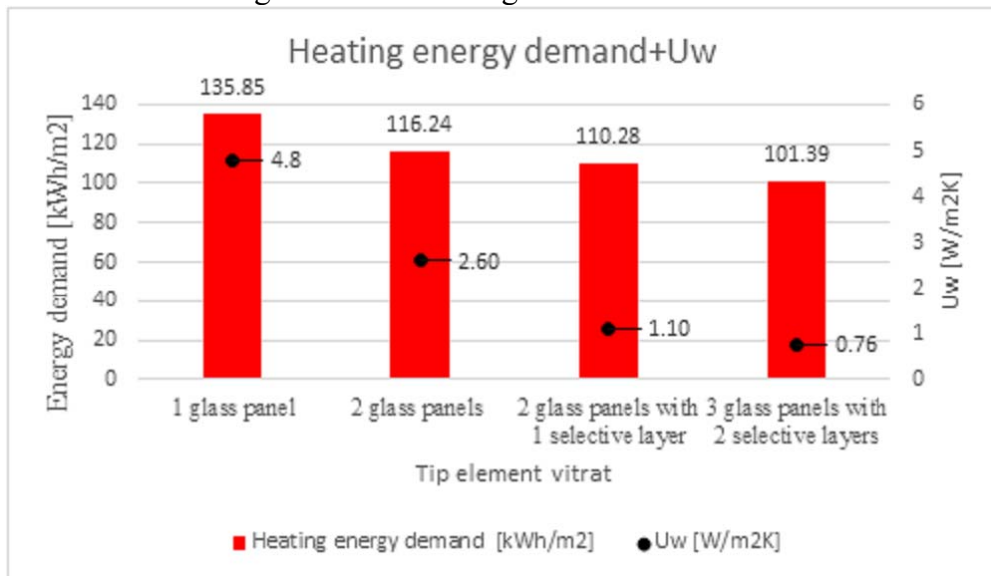


Fig.3. Heating energy demand + U_w graph

At the same time, the energy requirement for cooling, in the case of double-glazed windows without a selective layer (case 1, $g = 0.78$) decreases insignificantly,

by about 2 %, but the presence of a selective layer (case 2, $g = 0.38$) leads to a decrease of 37.8 %. Thus, the importance of reducing solar contributions during the summer is highlighted, in order to avoid overheating of living spaces. The triple glazing with 2 selective layers (case 3, $g = 0.40$) leads to a decrease in the cooling requirement of 34.4 % compared to the initial situation, but is about 3 % more than in case 2.

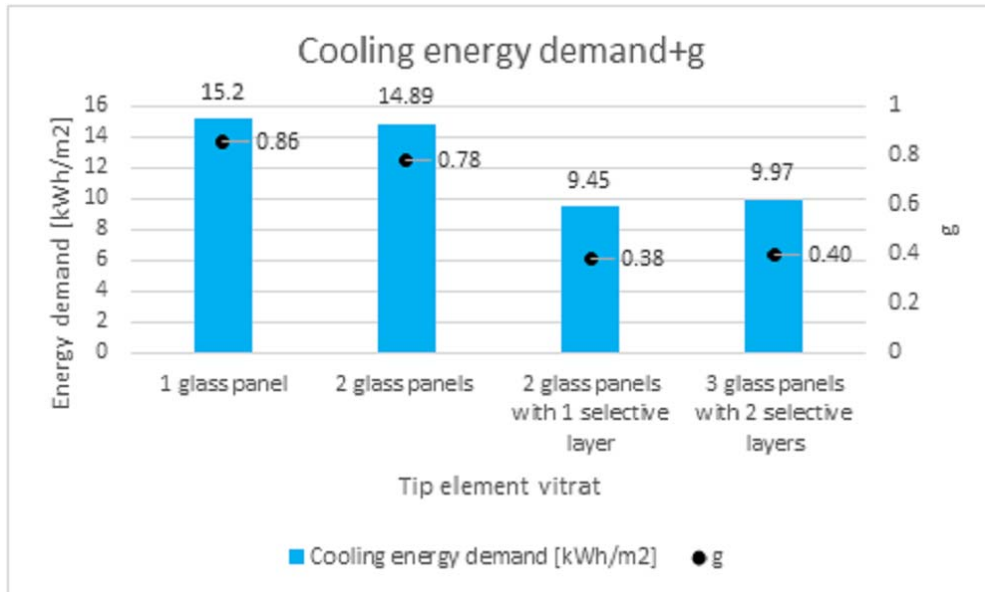


Fig.4. Cooling energy demant + g graph

The financial analysis has been carried out in order to determine whether the proposed investments are profitable and can be repaid within a reasonable period of time. We consider two situations from which we start:

- situation 1: we assume that the whole building has windows with a glass panel;
- situation 2: we assume that the whole building has windows with two glass panels.

The data entered as well as the payback periods of the investments are presented in the following table:

Table 2

Investment recovery time						
Case	Glazed element type	Energi saving S1 [kWh/m ²]	Energi saving S2 [kWh/m ²]	Cost [lei/m ²]	Investment recovery time S1 [ani]	Investment recovery time S2 [ani]
Initial situation	1 glass panel	-	-			
Case 1	2 glass panels	19.92	-	480.00	8.23	-

Case 2	2 glass panels with 1 selective layer	31.32	11.40	720.00	7.94	16.31
Case 3	3 glass panels with 2 selective layers	39.69	19.77	912.00	7.92	13.27

In situation 1, we start from the hypothesis that the existing block has single glazed windows and we analyze the investments related to the double glazing (case 1), double glazing with selective coating (case 2) and triple glazing with two selective layers (case 3). Following the evaluation of the economic indicators, for case 1 there is an investment recovery time of 8.23 years and 7.94 and 7.92 years for case 2 and 3 respectively. All 3 cases studied are financially efficient, the investment being recovered over the life of the glazed elements (20 years). Even if the lifespan of the windows would be shorter (10-15 years), any of the 3 options would be suitable. This evolution is shown in the following graph:

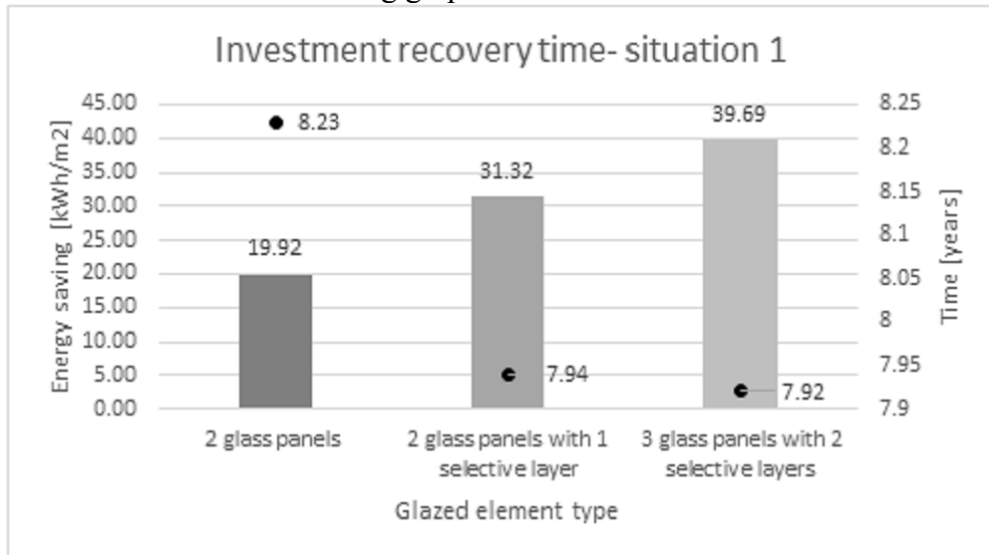


Fig. 5. Investment recovery time – situation 1

In situation 2, it is assumed that the existing block is already equipped with double glazed windows and the investments related to the double glazing with selective layer (case 2) and the triple glazing with two selective layers (case 3) are analyzed. In case 2, the recovery of the investment takes place in 16.31 years, and in case 3, in 13.27 years. Case 2 is only financially effective if the life of the glazed elements is 20 years. Perhaps a good option in this case would be to improve by adding a selective coated glass sheet and not completely replace the glazed elements. At the same time, case 3 is feasible even for a period of 15 years of glazed elements. This evolution is shown in the following graph:

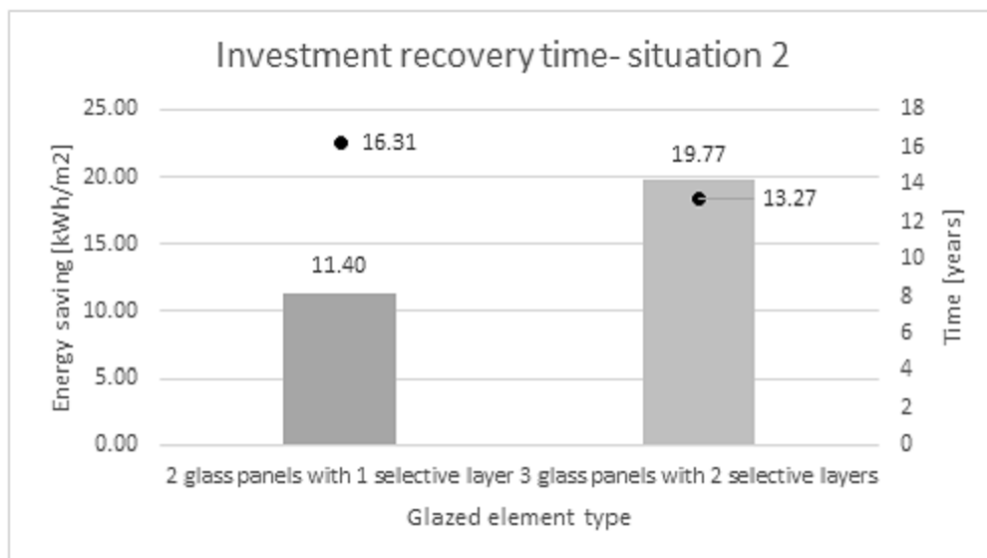


Fig. 6. Investment recovery time – situation 2

4. Conclusions

Nowadays, the energy rehabilitation of buildings is a preventive action, which is becoming more and more necessary to increase the sustainability of our cities [7]. This paper brings to the fore the importance of glazed elements in the energy performance of a building, by measuring and studying some parameters:

- full solar spectrum: UV, visible and IR rays;
- solar heat gain coefficient;
- heat transfer coefficient;
- tightness of glazed elements.

Their influence can be quantified in reducing the need for heat by using glazed elements with high thermal resistance given by multiple glazing and gas layers [8]. Moreover, the supply of seals considerably reduces air infiltration and at the same time the energy required for heating. This is highlighted in the case study presented in Chapter 4. At the same time, the glazed elements have a significant contribution in reducing the need for cooling. The use of glass with a high solar heat gain coefficient (g) corresponds to high solar inputs, which is beneficial in winter, but which can cause overheating in summer. Reducing the solar heat gain coefficient by applying selective layers on glass sheets leads to a decrease in solar inputs, as highlighted in the case study. The case study presents the importance of the parameters of the glazed elements justified by the energy efficiency, but also by the financial efficiency.

The author considers that special attention should be paid to the choice of glazed elements of buildings. A type of glazed element suitable for the climatic zone and the chosen orientation can only bring benefits, from the reduction of energy costs to the pleasant sensation produced by natural light.

References

- [1] *D.A. Pohoryles, C. Maduta, D.A. Bournas, L.A. Kouris*, Energy performance of existing residential buildings in Europe: A novel approach combining energy with seismic retrofitting, *Energy and Buildings*, Volume 223, 2020, 110024, ISSN 0378-7788, <https://doi.org/10.1016/j.enbuild.2020.110024>
- [2] *He Q, Ng ST, Hossain MU, Skitmore M*, Energy-Efficient Window Retrofit for High-Rise Residential Buildings in Different Climatic Zones of China. *Sustainability*. 2019; 11(22):6473. <https://doi.org/10.3390/su11226473>
- [3] *Maureen de Gastines, Andrea Elvira Pattini*, Window energy efficiency in Argentina Determining factors and energy savings strategies, *Journal of Cleaner Production*, Volume 247, 2020, 119104, ISSN 0959-6526, <https://doi.org/10.1016/j.jclepro.2019.119104>
- [4] *P T H Ha*, Energy efficiency façade design in high-rise apartment buildings using the calculation of solar heat transfer through windows with shading devices, *IOP Conf. Ser.: Earth Environ*, <https://doi.org/10.1088/1755-1315/143/1/012055>
- [5] Mc 001/1 – 2006 - Metodologie de calcul al performanței energetice a clădirilor. Partea I – Anvelopa clădirii;
- [6] ISO 9050 – 2012 – Glass in building – Determination of light transmittance, solar direct transmittance, total solar energy transmittance, ultraviolet transmittance and related glazing factors;
- [7] *Greca, Paolo & Margani, Giuseppe*, (2018). Seismic and Energy Renovation Measures for Sustainable Cities: A Critical Analysis of the Italian Scenario. *Sustainability*. 10. 10.3390/su10010254.
- [8] *Meng, Deming & Li, Bing & Zeng, Meng & Li, Chen & Dai, R.*, (2014). Study on Optical and Thermal Properties of Low-E Glass. *Advanced Materials Research*. 1035. 458-463. [10.4028/www.scientific.net/AMR.1035.458](https://doi.org/10.4028/www.scientific.net/AMR.1035.458).

Influența factorilor de ventilare asupra dezvoltării incendiilor în încăperi și clădiri. Recenzie studii numerice

The influence of ventilation factors on the development of fires in rooms and buildings. Review of numerical studies

Iulian-Cristian ENE^{1,3}, Vlad IORDACHE², Alexandru-George BECHERU³

¹Technical University of Civil Engineering of Bucharest
Str. Pache Protopopescu, no. 66, sector 2, Bucharest, Romania
iuliancristianene@gmail.com

²Technical University of Civil Engineering of Bucharest
Str. Pache Protopopescu, no. 66, sector 2, Bucharest, Romania
viordach@yahoo.com

³Police Academy – Fire Officer Faculty
Str. Morarilor, no. 3, sector 2, Bucharest, Romania
becheru_alex@yahoo.com

DOI: 10.37789/rjce.2023.14.2.4

Rezumat. *Ventilarea incendiilor reprezintă o procedură activă de intervenție care determină scăderea temperaturilor, concentrațiilor produșilor de ardere și creșterea vizibilității pentru facilitarea intervenției pompierilor în scopul salvării de vieți și de reducere a pagubelor materiale. În acest scop, a fost realizat un studiu bibliografic a cercetărilor experimentale și numerice inițiate în domeniul ventilării incendiilor. În urma consultării studiilor s-a evidențiat eficiența ventilării incendiilor pentru reducerea concentrațiilor produșilor de ardere și a temperaturii maxime și creșterea vizibilității. De altfel, pentru clădirile înalte s-a confirmat că ventilarea incendiului este puternic influențată de efectul de coș apărut din cauza diferențelor mari de nivel.*

Cuvinte cheie: ventilare, incendiu, temperatura, modelare numerică

Abstract. *Fire ventilation is an active intervention procedure that lowers temperatures, concentrations of combustion products and increases visibility to facilitate the intervention of firefighters for saving lives and reduce material damage. For this purpose, a bibliographic study of the experimental and numerical researches initiated in the field of fire ventilation was carried out. After consulting the studies, the efficiency of fire ventilation was highlighted for reducing the concentrations of combustion products and the maximum temperature and increasing visibility. Moreover, for high-rise buildings, it was confirmed that fire ventilation is strongly influenced by the stack effect caused by big level differences.*

Key words: ventilation, fire, temperature, numerical modelling

1. Introduction

In 2018 alone, fires incidents in the United States caused more than 2,700 deaths and 11,000 fire related injuries [1], meaning that one fire incident occurs among 906 people with a death rate per million of 8.19, the probability of that fire to cause injuries and/or deaths being approximately 3% and 0.7% respectively, and from the point of view, for the year 2018 as well, material losses were evaluated at more than 8 billion dollars, which means on average about 22,000 dollars equivalent of the damages produced by each fire. Also, for the United States of America, the mortality rate remained at a high value, both for professional fire-rescue teams, 2.51% of the total annual deaths [2]–[4], as well as for the American civilian population [5]–[7].

In the case of the states of the European Union, although the mortality rate caused by fires was in a continuous decrease after 1988 as a result of the common European fire incidents prevention policy, but its value continues to remain quite high even after the year 2000, many states not providing data on such events [8]. In the UK since 2000 mortality has fallen considerably, falling by at least 50% in 2016 due to increased use of residential smoke detectors [9].

Therefore, to reduce the incidence of deaths caused by fire and to increase the fire safety of buildings, after the year 2000 at the global level, a series of experimental and numerical studies in the field of fire security were started. I have chosen to consult predominantly numerical scientific papers because they can be reinitialized many more times than experimental ones, much easier and with less resource consumption. Hence, through this paper, following the detailed consultation of scientific works in the field of fire ventilation, we proposed the analysis of numerical fire studies, based rooms or buildings models, the study of fire development for different types of combustible materials, the study of the influence of ventilation conditions on the development of fires, studying smoke exhaust and active and passive ventilation systems, their specifications and how to use them for the purpose of the buildings in which they were installed, as well as making a record of the equipment used from the papers consulted, in conjunction with the presentation of new numerical research directions at the present time in the field of fire security.

In the multitude of these different types of research, numerical and experimental, there is a need to conduct a review-type study regarding the main directions of fire security research, fire security equipment in modern buildings and the influence of this equipment on the development of fire incidents and the safety of the population affected by this type of risk.

2. Numerical studies in the field of fire ventilation

Fire ventilation or operational ventilation involves the active and controlled change of conditions in a burning room or building to evacuate smoke and hot gases in order to reduce the temperature and increased concentrations of combustion products, facilitating the evacuation of occupants and the intervention of firefighters (Fig. 1).



Fig. 1. Natural ventilation [10]

Although in some cases the initiation of operational ventilation can lead to a local increase in temperature, even an incorrectly performed fire ventilation procedure is recommended to the detriment of its absence [11]. This method of extinguishing the fire without using operational ventilation in any way can be found in the specialized literature under the name of anti-ventilation. Fire ventilation can be passive, active or hybrid, and from the point of view of efficiency, both active and hybrid operational ventilation cause an easier intervention for the fire brigades, the fire is located at the level of a single room, the temperature is kept high yet controlled and, thanks to the supply of oxygen brought by ventilation, incomplete combustion is almost non-existent, reducing the concentration of carbon monoxide and other flammable gases [12].

Frederick W. Mowrer through the research he started [13] provided a starting point for understanding the factors that determine and influence the movement of smoke and hot gases. In this study, not only the driving forces that determine the movement of smoke were targeted, but also the smoke detection and exhaust systems that are commonly used to control the movement of smoke within buildings and other spaces. These factors have been addressed individually and conclusions have been drawn for each factor separately, but it is highlighted that for some practical applications it will be necessary to use simulation software that takes into account the combined effects of these factors. A series of design problems of smoke exhaust systems were addressed in a general way, requiring a more detailed analysis,

Following the same research direction from previous years [14]–[16], Lulea et. al. carried out a research by developing a CFD model to create an interdependence between the operation of the sprinkler system and the operation of the ventilation system [17]. A full-scale experiment was conducted and a CFD model was developed. The thermal conductivity of the experimental test stand walls, domain refinement and burner HRR variation were introduced as model inputs so that the resulting time variation of the temperature near the sprinkler location corresponded to the actual measured variation. Two other experiments contributed to the validation of the numerical model. In addition to the air temperature, at a given time, other essential

parameters inside the stand were determined such as the ambient air temperature, visibility, oxygen concentration and carbon dioxide concentration. As a result of the research, it was concluded that if the ventilation speed increases, the internal temperatures in the outbreak area decreases, and the sprinkler for that area is activated with a delay or not at all. However, this conclusion is not universally valid for the entirety of the analyzed experimental stand, since the ventilation system, along with the natural air movement, implies a specific air speed and a specific temperature distribution inside the analyzed space.

Starting from a previous experimental research [18], Cai N. and Chow WK performed FDS-type numerical modelling to determine solutions of two existing problems at the time, the feasibility of defined boundary conditions and determining the optimal refinement to obtain the most relevant results [19]. The numerical model created aimed to study the influence upon the height of the ventilation gap (door) in 3 scenarios: the fully open door (SC1), the door open at the lower half (SC2) and the door open at the lower quarter (SC3), and at two domains with different dimensions and refinements (OB1 and OB2), as it can also be seen from Fig. 2.

Analysing the results of the simulations from a functional point of view, the Euclidean norm (the difference between the lengths of pressure vectors) and the cosine of the angle formed by two vectors (a comparison of curves shapes) are used to compare the numerical results obtained from the FDS model with the experimentally measured data. For a better accuracy of the two curves from experiment and model, the norm is expected to approach 0, and the cosine is expected to approach 1 [20].

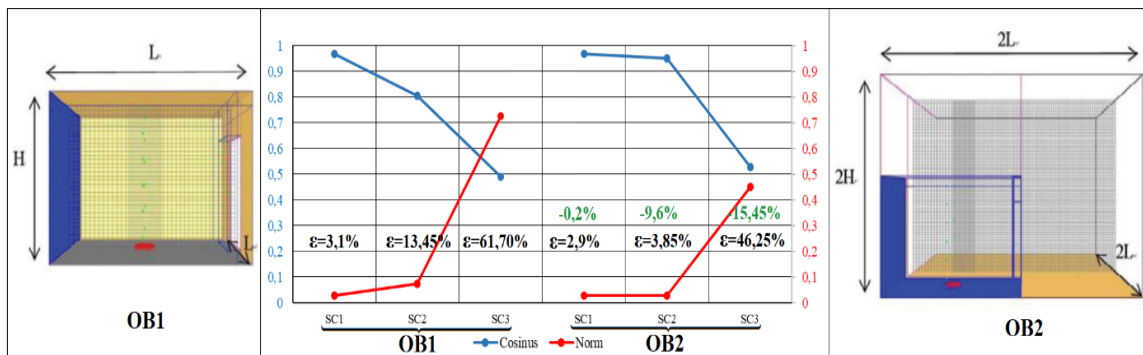


Fig. 2. Analysis of the influence of domain and ventilation conditions on simulation results [19]

It can be seen from Fig. 2 that, with the 8-fold increase in domain size and refinement, the average error between the experimental and numerical model results was reduced by up to -0.2% for SC1, -9.6% for SC2 and -15.45% for SC3, drawing the conclusion that a larger and more refined domain leads to more feasible numerical results independent of the chosen ventilation conditions.

Continuing the research direction started by the previously presented studies [21], [22], Panindre et. al. [23] and Kuti et. al. [24], carried out two simulations to determine the optimal distance of the operational fan from the building's main entrance and implicitly the dimensions of its reducer, which in the specialized field is used to obstruct part of the surface of the ventilation gap in order to limit the occurrence of multiple-way smoke circulation (Door Open Area Reducer or DOAR). Two scenarios were studied using a DOAR only, or in its absence. The temperature inside the building was monitored in relation to the height between the upper end of the fan and the lower side of the DOAR (k) and the distance from the fan to the entrance of the building (w). These numerical studies developed and highlighted the concept of ventilation by creating a positive pressure (overpressure inside the room) that causes the smoke to be evacuated from the room more quickly. As a result of the two numerical modelling, it was found that the optimal distance for the fan location is between 0.9-1.2 m.

In 2017, following the study of some experiments carried out by NIST [21], [25], Panindre et. al. performed a study based on a computer simulation in FDS [22], in this paper addressing the technical term positive pressure ventilation (PPV) for a fire in an apartment on the 5th floor of a high-rise building. The study demonstrates the efficiency of PPV in reducing temperatures and concentrations of toxic gases in the stairwell and hallway, key locations during the intervention of fire brigades. Six ventilation scenarios were introduced: natural ventilation (NO PPV), ventilation with one fan (PPV) and/or wind control device (WCD+PPV), ventilation with wind control device (WCD), ventilation with two fans located on floors 1 and 3 (2PPV) and ventilation with two fans located in parallel on floor 1 (P2-PPV). Moreover, the wind can also have a significant impact on the evolution of the fire, the influence of wind speed variation was studied at 2.5; 5; 7.5 and 10 m/s for the simulation under natural operational ventilation conditions and 7.5 and 10 m/s for the simulation under forced ventilation conditions by placing one or more operational fans at different levels and/or using a wind control (Fig. 3).

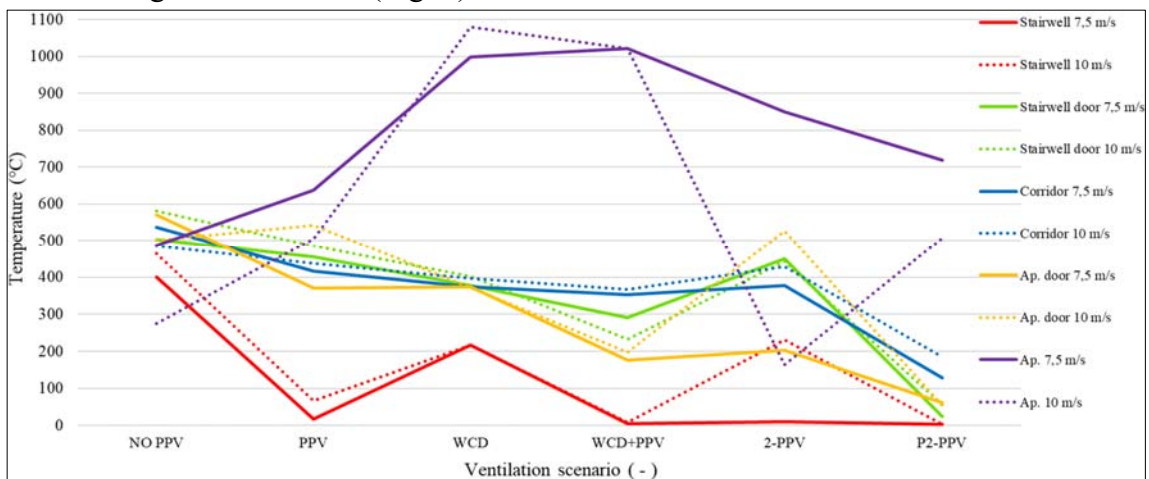


Fig. 3. Analysis of temperature according to ventilation scenarios and wind conditions [22]

In the Fig. 3 the temperature evolution in different locations was depicted depending on the ventilation scenario and the wind speed chosen. The ventilation efficiency is mainly determined by the temperature difference between two landmarks: the stairwell (red) and the burning apartment (purple). If in the case of natural ventilation, the temperature differences between the two benchmarks are around 100 °C, in the case of active ventilation scenarios this value exceeds 600 °C. It can also be seen that in all the active ventilation scenarios a considerably lower temperature is recorded compared to the natural ventilation scenario. Analysing all the ventilation scenarios, we can conclude that the most efficient ventilation method is the one with two fans located in parallel (P2-PPV).

Although the application of a ventilation tactic by creating overpressure inside the building reduces the risk of uncontrolled spread of smoke and flames, in high wind conditions its effectiveness decreases. In these cases where the wind has an important contribution to the fire development, the use of wind control devices (Wind control devices or WCD) simultaneously with the correct application of operational ventilation can significantly increase the pressure recorded inside the building, accelerating the evacuation of gases and reducing the released heat by fire and implicitly the temperatures inside the stairwell and in the hallways, these being the main points of interest during the intervention of the firefighters.

4. Analysis of the influence of ventilation conditions and the stack effect on the fire evolution

The results of the previously studied papers showed a considerable influence of the ventilation conditions on the fire development. Whether we refer to the nature of the ventilation, the environmental conditions or the equipment used, all these have an important impact on the speed of fire spread and the temperatures recorded inside the burning space. Moreover, the stack effect has an important contribution to increasing the speed of fire spread, the influence of this factor increasing exponentially with the height of the burning building.

For studying the influence of ventilation conditions on temperature, the results obtained from 5 studies were compared below. The study of these scientific papers was carried out with the aim of analysing in terms of quality the effectiveness of deliberate ventilation of fires at the expense of faulty ventilation or even its absence, certain input data such as the characteristics of the outbreak, the ventilation conditions, the geometry of the numerical model, the refinement of the domain and the atmospheric conditions do not have close values. It was observed that following the analysis of the 5 numerical studies, the same conclusion can be stated in general, specifically that the ventilation of a fire causes a decrease in the T_{MAX} value by up to 73%, as it can also be seen from the results presented in *Table 1*.

Table 1

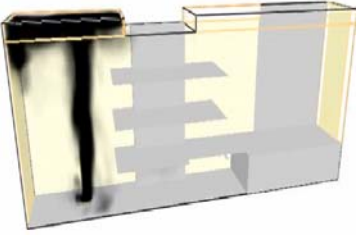
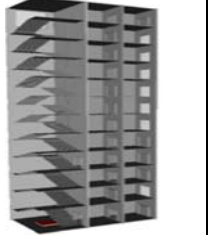
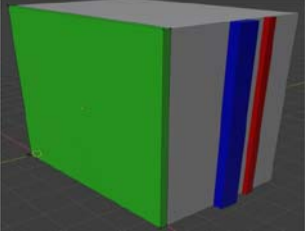
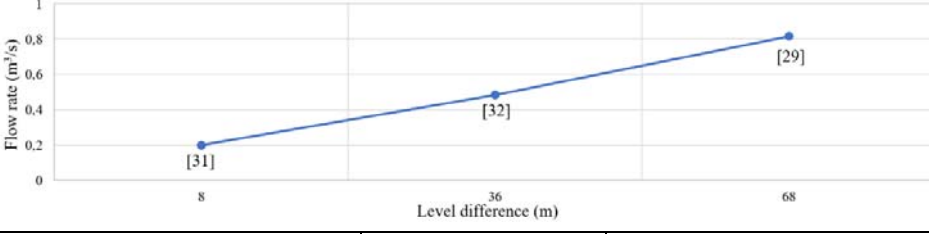
Influence of ventilation conditions on temperature					
Studies	[26]	[27]	[28]	[22]	[24]
Comparative analysis of T_{MAX} for non-ventilated/ventilated fires	<p>Temperature (°C)</p> <p>Legend: Non-ventilated fire (blue), Ventilated fire (orange)</p> <p>Percentage differences: -35,55%, -36,53%, -63,46%, -66,49%, -73,19%</p>				
	Ventilation type / ACH	Exhaust Fan 1 h ⁻¹	Natural Ventilation	Intake Fan (PPV) 45,37 h ⁻¹	Intake Fan (PPV) 12,22 h ⁻¹
T_{MAX} non-ventilated fires	225 °C	1300 °C	323 °C	1143 °C	235 °C
T_{MAX} ventilated fires	145 °C	825 °C	118 °C	383 °C	63 °C
ΔT_{MAX}	80 °C -35,55%	475 °C -36,53%	205 °C -63,46%	760 °C -66,49%	172 °C -73,19%

where, ACH represents air change per hour, T_{MAX} represents the maximum temperature measured inside the burning space, and ΔT_{MAX} represents the temperature difference between two compared situations, when the fire is non-ventilated and ventilated.

In order to study the stack effect in high-rise buildings, several studies were consulted in which different software were used, FireSTORM [29], COSMO and CONTAM [30] and PyroSim [31], [32], following the main advantages and disadvantages of each. Moreover, in order to understand the stack effect phenomenon, experimental studies started in this regard were also consulted [30], [33]–[36] concluding that a faithful experimental representation of the stack effect cannot be reproduced by a small-scale experiment. If we refer to tall and very tall buildings, the stack effect is much more present due to the considerable height of vertical gaps, stairwells and elevator shafts.

Analysing the influence of this effect on the speed of fire spread and the speed of smoke flow, it was observed that, for tall and very-tall buildings, the increase in the number of floors from 3 to 17 implies amplifying the fire by 4-5 times. For a level difference of 8 m, the measured flow velocities were around 2 m/s most of the time, at an air flow rate of 0.2 m³/s. The air flow velocity values varied depending on the size of the ventilation gap between 2 and 4 m/s according to Fig. 3 of [31]. The increase in the level difference to 36 m determined an appreciation of the air flow volume up to the value of 0.484 m³/s. Later, comparing these results with those of the third study, it was observed that the air mass flow rate increased to the value of 1 kg/s (approximately 0.816 m³/s), causing an increase compared to the first situation by up to 208% (Table 2). The data entered in the table resulted from studying the graphs of the *Cold ffl* case according to Fig. 9 (a) of [29], the difference between the maximum and minimum value tended to 1 kg/s.

The influence of the stack effect on fire development

Studies	[31]	[32]	[29]												
Numerical model															
Evolution of the flow rate depending on the height	 <table border="1"> <caption>Data for Flow rate vs Level difference</caption> <thead> <tr> <th>Level difference (m)</th> <th>Flow rate (m³/s)</th> <th>Study</th> </tr> </thead> <tbody> <tr> <td>8</td> <td>0.2</td> <td>[31]</td> </tr> <tr> <td>36</td> <td>0.484</td> <td>[32]</td> </tr> <tr> <td>68</td> <td>0.816</td> <td>[29]</td> </tr> </tbody> </table>			Level difference (m)	Flow rate (m³/s)	Study	8	0.2	[31]	36	0.484	[32]	68	0.816	[29]
Level difference (m)	Flow rate (m³/s)	Study													
8	0.2	[31]													
36	0.484	[32]													
68	0.816	[29]													
V_{MAX}	2 m/s	2,18 m/s	4,18 m/s												
Z	8 m (3 floors)	36 m (12 floors)	68 m (17 floors)												
$\dot{V}_{MAX}, \Delta\dot{V}_{MAX}$	0,2 m³/s	0,484 m³/s, +142%	0,816 m³/s, +308%												

where, V_{MAX} represents air velocity, \dot{V}_{MAX} represents the volume flow of air in the building, and $\Delta\dot{V}_{MAX}$ represents the difference between two compared situations, [31] with [32] and [31] with [29].

5. Conclusions

The fire ventilation procedure, used properly, determines an easier and safer intervention for the firefighters. As presented in the previously mentioned studies, a non-ventilated fire compared to a ventilated one, due to the stratification and stagnation of smoke, generates a higher temperature throughout the building, while the ventilated fire, natural (passive) or forced (active), will cause a high temperature only within the burning compartment, in the rest of the rooms the temperatures being lower by up to 70%. In addition to the temperature, the effectiveness of the application of fire ventilation tactics was also confirmed in reducing the concentrations of combustion products such as monoxide and carbon dioxide and by increasing visibility, both factors being very important in facilitating the self-evacuation of the occupants of the respective space.

Moreover, for tall and very tall buildings, it was proven, through this research, that fire ventilation is strongly influenced by the stack effect caused by large differences in level, therefore research in this direction is feasible on the conditions of increasing the number of this type of buildings worldwide. The stack effect, along with the increase in the level difference, causes an exponential increase in the flow speed of the air currents. The stack effect causes an intake of air to be drawn to the level of the lower floors and thus, the fire started on a higher floor is continuously supplied with oxygen.

The perspective of studying the stack effect and the overpressure ventilation (PPV) technique profiles a need to start numerical studies in this new direction. In the previously mentioned articles, usually only 1-2 parameters were monitored, predominantly temperature and pressure, but there are others that can provide information on the interdependence between the level difference and other parameters associated with the fire.

Only the continuous study of smoke removal and operational ventilation can lead to innovation in the field of fire security of buildings, a very important feature to significantly reduce the loss of human life, material losses generated by fire and pollution in the urban environment.

References

- [1] N. A. of S. F. S. Brushlinsky, M. N. F. P. A. Ahrens, S. A. of S. F. S. Sokolov, and P. B. F. and R. A. Wagner, "World Fire Statistics," *Int. Assoc. Fire Rescue Serv.*, vol. 23, 2018.
- [2] R. F. Fahy, P. R. LeBlanc, and J. L. Molis, "FIREFIGHTER FATALITIES IN THE UNITED STATES – 2009," *Natl. Fire Prot. Assoc. Fire Anal. Res. Div.*, 2010, [Online]. Available: https://www.usfa.fema.gov/downloads/pdf/publications/ff_fat09.pdf.
- [3] U.S. Department of Homeland Security, "Firefighter Fatalities in the United States in 2018," Emmitsburg, MD 21727, 2019. [Online]. Available: https://www.usfa.fema.gov/downloads/pdf/publications/firefighter_fatalities_2018.pdf.
- [4] U. S. F. Administration, *Fire Death Rate Trends; An International Perspective*. Fema.
- [5] U.S. Fire Administration, "Fire Death Rate Trends: An International Perspective," Emmitsburg, Maryland 21727, 2007. [Online]. Available: <https://www.modernbuildingalliance.eu/assets/uploads/2018/05/Fire-Death-Rate-Trends-An-International-Perspective.pdf>.
- [6] N. F. P. A. Marty Ahrens, "Home Structure Fires," *NFPA Res.*, 2019.
- [7] N. F. P. A. Marty Ahrens, "Home Structure Fires Supporting Tables," *NFPA Res.*, vol. 10, 2019.
- [8] Mif. M. Kobes, MSc, BBE, Ms. K. Groenewegen - Ter Morsche, and D. M. G. Duyvis, "European statistics and potential fire safety measures," Arnhem, 2009. [Online]. Available: https://www.ifv.nl/kennisplein/Documents/09-06-24_rapport_consumer_fire_safety_pdf1.pdf.
- [9] Stephanie Bryant and Isabel Preston, "Focus on trends in fires and fire-related fatalities," London, 2017. doi: ISBN: 978-1-78655-5717.
- [10] Ottawa Fire Services, "Fire Assessment Guide," *Structural firefighting*. [Online]. Available: <https://guides.co/g/fa204-fire-assessment-sd/>.
- [11] L. J. Li, F. Tang, M. S. Dong, and C. F. Tao, "Effect of ceiling extraction system on the smoke thermal stratification in the longitudinal ventilation tunnel," *Appl. Therm. Eng.*, vol. 109, pp. 312–317, Oct. 2016, doi: 10.1016/J.APPLTHERMALENG.2016.08.071.
- [12] F. Tang, L. J. Li, M. S. Dong, Q. Wang, F. Z. Mei, and L. H. Hu, "Characterization of buoyant flow stratification behaviors by Richardson (Froude) number in a tunnel fire with complex combination of longitudinal ventilation and ceiling extraction," *Appl. Therm. Eng.*, vol. 110, pp. 1021–1028, Jan. 2017, doi: 10.1016/J.APPLTHERMALENG.2016.08.224.
- [13] F. W. Mowrer, "Driving Forces for Smoke Movement and Management," *Fire Technol.*, vol. 45, no. 2, pp. 147–162, 2009, doi: 10.1007/s10694-008-0077-1.
- [14] E. Guillaume, F. Didieux, A. Thiry, and A. Bellivier, "Real-scale fire tests of one bedroom apartments with regard to tenability assessment," *Fire Saf. J.*, vol. 70, pp. 81–97, 2014, doi: <https://doi.org/10.1016/j.firesaf.2014.08.014>.

- [15] Y. Tong, D. Huo, P. Zhu, and X. Niu, "Prediction of natural and hybrid ventilation performance used for fire-induced smoke control in a large single space," *Fire Saf. J.*, vol. 100, pp. 20–31, 2018, doi: <https://doi.org/10.1016/j.firesaf.2018.03.005>.
- [16] X. Jiang, G. Zhu, H. Zhu, and D. Li, "Full-scale Experimental Study of Fire Spread Behavior of Cars," *Procedia Eng.*, vol. 211, pp. 297–305, 2018, doi: <https://doi.org/10.1016/j.proeng.2017.12.016>.
- [17] M. D. Lulea, V. Iordache, and I. Nastase, "Numerical Model Development of the Air Temperature Variation in a Room Set on Fire for Different Ventilation Scenarios Marius Dorin Lulea, Vlad Iordache * and Ilinca Năstase," *Appl. Sci.*, vol. 11, p. 11698, 2021, doi: [10.3390/app112411698](https://doi.org/10.3390/app112411698).
- [18] W.K. Chow, G. W. Zou, Y. Gao, and N. Zhu, "Experiment on room fire with oxygen consumption calorimetry," *Int. J. Eng. Perform. - bases code*.
- [19] N. Cai and W. K. Chow, "Air Flow through the Door Opening Induced by a Room Fire under Different Ventilation Factors," *Procedia Eng.*, vol. 43, pp. 125–131, 2012, doi: <https://doi.org/10.1016/j.proeng.2012.08.022>.
- [20] R. Peacock, P. Reneke, W. Davis, and W. Jones, "Quantifying Fire Model Evaluation Using Functional Analysis," 1999, [Online]. Available: https://tsapps.nist.gov/publication/get_pdf.cfm?pub_id=913096.
- [21] D. Madrzykowski and S. Kerber, "Fire Fighting Tactics Under Wind Driven Fire Conditions: 7-Story Building Experiments." Technical Note (NIST TN), National Institute of Standards and Technology, Gaithersburg, MD, 2009, [Online]. Available: https://tsapps.nist.gov/publication/get_pdf.cfm?pub_id=902177.
- [22] P. Panindre, N. S. S. Mousavi, and S. Kumar, "Positive Pressure Ventilation for fighting wind-driven high-rise fires: Simulation-based analysis and optimization," *Fire Saf. J.*, vol. 87, pp. 57–64, 2017, doi: <https://doi.org/10.1016/j.firesaf.2016.11.005>.
- [23] P. Panindre, N. S. S. Mousavi, and S. Kumar, "Improvement of Positive Pressure Ventilation by optimizing stairwell door opening area," *Fire Saf. J.*, vol. 92, pp. 195–198, 2017, doi: <https://doi.org/10.1016/j.firesaf.2017.06.007>.
- [24] R. Kuti, G. Zolyomi, and O. Kegeyes-Brassai, "Assessing the impact of positive pressure ventilation on the building fire - A case study," *Int. J. GEOMATE*, vol. 15, pp. 16–21, Aug. 2018, doi: [10.21660/2018.48.18042](https://doi.org/10.21660/2018.48.18042).
- [25] D. Madrzykowski, S. Kumar, and Prabodh, "Wind, Fire, and High-Rise Buildings: Firefighters and Engineers Conduct Research to Combat a Lethal Threat." 2010, [Online]. Available: https://tsapps.nist.gov/publication/get_pdf.cfm?pub_id=905582.
- [26] S. Brohez and I. Caravita, "Fire induced pressure in airtight houses: Experiments and FDS validation," *Fire Saf. J.*, vol. 114, p. 103008, Jun. 2020, doi: [10.1016/j.firesaf.2020.103008](https://doi.org/10.1016/j.firesaf.2020.103008).
- [27] S. Kerber, "Analysis of One and Two-Story Single Family Home Fire Dynamics and the Impact of Firefighter Horizontal Ventilation," *Fire Technol.*, vol. 49, no. 4, pp. 857–889, 2013, doi: [10.1007/s10694-012-0294-5](https://doi.org/10.1007/s10694-012-0294-5).
- [28] S. Svensson, "Experimental Study of Fire Ventilation During Fire Fighting Operations," *Fire Technol.*, vol. 37, no. 1, pp. 69–85, 2001, doi: [10.1023/A:1011653603104](https://doi.org/10.1023/A:1011653603104).
- [29] S. Bilyaz, T. Buffington, and O. Ezekoye, "The Effect of Fire Location and the Reverse Stack on Fire Smoke Transport in High-Rise Buildings," *Fire Saf. J.*, p. 103446, Sep. 2021, doi: [10.1016/J.FIRESAF.2021.103446](https://doi.org/10.1016/J.FIRESAF.2021.103446).
- [30] L. Wang, W. Z. Black, and G. Zhao, "Comparison of simulation programs for airflow and smoke movement during high-rise fires," *ASHRAE Trans.*, vol. 119, pp. 157–168, Jan. 2013.
- [31] R. Al-Waked, M. Nasif, N. Groenhout, and L. Partridge, "Natural ventilation of residential building Atrium under fire scenario," *Case Stud. Therm. Eng.*, vol. 26, p. 101041, Aug. 2021, doi: [10.1016/J.CSITE.2021.101041](https://doi.org/10.1016/J.CSITE.2021.101041).
- [32] G. Zhao, T. Beji, and B. Merci, "Study of FDS simulations of buoyant fire-induced smoke movement in a high-rise building stairwell," *Fire Saf. J.*, vol. 91, pp. 276–283, Jul. 2017, doi: [10.1016/J.FIRESAF.2017.04.005](https://doi.org/10.1016/J.FIRESAF.2017.04.005).

- [33] W. Shi, J. Ji, J. Sun, S. Lo, L. Li, and X. Yuan, “Experimental Study on the Characteristics of Temperature Field of Fire Room under Stack Effect in a Scaled High-rise Building Model,” *Fire Saf. Sci.*, vol. 11, pp. 419–431, Jan. 2014, doi: 10.3801/IAFSS.FSS.11-419.
- [34] J. He, X. Huang, X. Ning, T. Zhou, J. Wang, and R. Yuan, “Stairwell smoke transport in a full-scale high-rise building: Influence of opening location,” *Fire Saf. J.*, p. 103151, Aug. 2020, doi: 10.1016/j.firesaf.2020.103151.
- [35] D. Qi, L. Wang, and R. Zmeureanu, “An Analytical Model of Heat and Mass Transfer through Non-adiabatic High-rise Shafts during Fires,” *Int. J. Heat Mass Transf.*, vol. 72, pp. 585–594, May 2014, doi: 10.1016/j.ijheatmasstransfer.2014.01.042.
- [36] H. Sha, X. Zhang, X. Liang, and D. Qi, “Reduced-scale experimental and numerical investigation on the energy and smoke control performance of natural ventilation systems in a high-rise atrium,” *E3S Web Conf.*, vol. 356, p. 2010, Aug. 2022, doi: 10.1051/e3sconf/202235602010.

Optimizarea termodinamica a unui sistem hibrid inovativ care utilizeaza captatoare solare si pompa de caldura pentru date climatice zilnice

Thermodynamic optimization of a novel hybrid system using solar collector and heat pump based on daily weather data

Florin IORDACHE¹, Mugurel TALPIGA²

^{1,2} Universitatea Tehnică de Construcții București
Bd. Lacul Tei nr. 122 - 124, cod 020396, Sector 2, București, România
E-mail: *fliord@yahoo.com*, *talpiga.mugurel@gmail.com*

DOI: 10.37789/rjce.2023.14.2.5

Rezumat. Lucrarea de fata prezinta un sistem termic hibrid inovativ compus din captatoare solare, robinet de reglaj proportional, rezervor de acumulare si pompa de caldura conectate hidraulic in serie, pentru a satisface necesarul de caldura al unei cladiri. Procedura evalueaza valoarea temperaturii de iesire a robinetului de reglaj, pentru a obtine temperatura proiectata la iesirea captatorilor solari, astfel incat energia acumulata peste zi in interiorul rezervorului de acumulare, sa satisfaca necesarul energetic la vaporizatorul pompei de caldura pentru a putea genera la condensator toata energia necesara pentru incalzire. Ecuatiile matematice sunt astfel propuse, precum si un algoritm de functionare, pentru a calcula temperatura de iesire a robinetului de reglaj in schema hidraulica propusa. In capitoul de concluzii, sunt prezentate avantajele acestui algoritm, prin plotarea rezultatelor simulate in diverse conditii climatice si de necesar termic de incalzire.

Cuvinte cheie: sistem hibrid, captatoare solare, necesar termic

Abstract. The paper presents a novel hybrid heating system composed by solar collectors, mixing valve, heat storage tank and heat pump hydraulically connected in series, to satisfy the heating demand of a building. The procedure evaluates the temperature set-point value of the mixing valve, to obtain the design output temperature of solar collector, thereby the energy accumulated over the day inside storage tank should satisfy required heat pump evaporator energy to deliver at its condenser building demand. Mathematical equations are thus proposed and algorithm to establish mixing valve temperature set-point is presented. In the conclusion of the paper are described advantages of this algorithm based on plotted simulation results in several weather conditions and building heating demands.

Keywords: hybrid system, solar collectors, thermal requirement

1. Introduction

Solar energy usage as an alternative to hydrocarbons start increase over past years. As a renewable resources as indirect energy source as solar radiation and indirect usage as environmental storage in air, rivers, lakes, underwater or ground, solar energy is part of our daily life. Responsible to drive all living creatures sun is used today for thermal comfort of humans during hot or cold season or for daily hot water preparation. Wide range of technologies to transfer or transform the solar energy to be used in heating or cooling demands are developed by today research and exploitation fields. Thermal solar collectors are ones must used equipment when solar radiation is the primary energy driven the system. In parallel, once vapor compression technology was developed, pressurized refrigerant properties are used by heat pumps to deliver thermal agents at a desired temperature potential useful to provide thermal comfort required by buildings.

By time, where proposed by research field, to be used a mix of technologies used in different thermal configurations, to satisfy the newly or rehabilitated buildings heating/cooling demand, to deliver a more efficient and sustainable thermal energy in a nature friendly mindset. This mix of technologies are commonly described today by the term hybrid systems, where at least two types of energies are used to satisfy building energy demand.

The mix of technologies helps decrease as much as possible equipment physical parameters and design requirements which can otherwise resulting in a more powerful equipment to satisfy the worst environment conditions demand but with high implementation cost and for a shortest period of time, when external weather conditions have very low apparition during the season. Thus, combining two or more technologies, can be drastically decreased the power of each equipment to deliver same amount of required energy to assure thermal comfort of final consumer.

2. System description

This paper presents a classical solar system composed by solar collectors and thermal storage tank for energy accumulation over the day. The novelty of this hydraulic diagram is the proportional mixing valve in the solar loop. With this connection, the output of solar collector thermal agent temperature can be controlled.

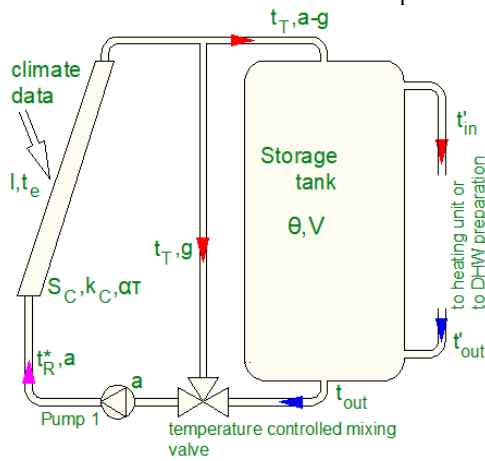


Fig 1

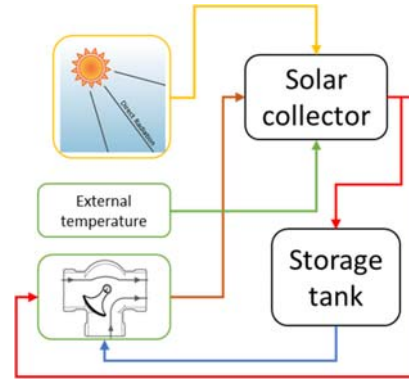


Fig 2

In figure 1 it is presented the hydraulic connection for solar loop in which solar collector input flowrate is constant over the time due to recirculating pump 1. Because the recirculating pump is installed after the proportional mixing valve, the flow in both valve inputs circuits is assured with only one pump. This is an advantage of the schematic which reduce the implementation and exploitation costs over the time. As can be seen on the notations, flow “a” is a constant value and g changes over time. Proportionality between the two inputs is assured by an electronic controller on which set temperature at output of mixing valve can be changed with values evaluated by mathematical model presented in this paper.

$$g = a \cdot \frac{t_R^* - t_{out}}{t_T - t_{out}} \quad (1)$$

Flow rate, g, in the high temperature input line of mixing valve is it directly evaluated knowing both inputs temperature of the proportional mixing valve. Thus, the hot input pipeline flow rate is evaluated with equation 1, where hot input line temperature, t_T , is the design temperature of solar collector output, cold line temperature, t_{out} , is the output temperature value from the bottom of the thermal energy storage tank, and proportional mixing valve temperature, t_R^* , being the set temperature for solar collector input.

Solar collector mathematical model design temperature is given by equation 2. Functionality of solar system witch collector is described by equivalent temperature, given by equation 4, and mechanical parameters evaluated with the thermal module, E, evaluated with equation 3.

$$t_T = t_E + (t_R^* - t_E) \cdot E \quad (2)$$

$$E = e^{-\frac{F' \cdot k_{\Sigma} \cdot S}{a \cdot \rho \cdot c}} \quad (3)$$

$$t_E = \frac{\alpha \cdot \tau}{k_c} \cdot I_{sol} + t_e \quad (4)$$

Setup temperature of mixing valve is the input temperature of solar collector, its value, external temperature value and solar radiation giving the inputs coefficients of solar system described by model in figure 2. For a given set of daily data, external temperature and solar radiation will assure the design temperature. This is possible by a specific input temperature, t_R^* , evaluated based on known data and design temperature at the solar collector output. Thus, rewriting equation 2 by equation 3, we can evaluate input temperature based on known external data and design temperature.

$$t_R^* = \frac{t_T - t_E \cdot (1 - E)}{E} \quad (5)$$

Inside energy storage tank the temperature follows a thermocline profile with hot temperature at the top of the tank and cold temperature at the bottom of it. By design, hot temperature is design temperature, t_T , of solar collectors, and cold temperature, t_{out} , is the initial temperature before starting the solar collector functional period. The simulation of thermal storage tank is realized with a pre-trained neural network with 90 neurons on hidden layer, analyze presented before in the research. Condition of storage tank functionality is energy saturation inside tank should not be realized, thus, the output temperature of bottom volume of tank is constant over the time and cold input line of proportional mixing valve it easy to simulate.

Heat pump model consist of isentropic efficiency applied to Carnot efficiency between evaporation and condensing temperatures based on equation 6.

$$Q_{cd} = \eta_{el} \cdot f_{cd} \cdot \frac{t_{cd} + \Delta t_{cd} + 273.15}{t_{cd} - t_T + \Delta t_{cd} + \Delta t_{vp}} \cdot W_{comp} \quad (6)$$

Condensing equivalence factor, f_{cd} , is a form of Carnot efficiency evaluated by simulation and consist in polynomial regression calculation of its value. In the paper was presented a 3x2 regression coefficient matrix representation and two more matrixes, one used for evaporator temperature and the other for condensing temperature. Thus, in a mathematical simulation tool like Matlab, a matrix form of equation coefficients are convenient to be used. Compressor electrical engine efficiency, η_{el} , reduce compressor power applied to condensing Coefficient of Performance, COP_{cd} , based on manufacturer datasheets. Heat pump evaporator temperature is the designed temperature of solar collector temperature with its value

conditions presented in this paper. Condensing and evaporation temperature differences, Δt_{cd} and Δt_{vp} , represent design values of this coefficient, to satisfy heat transfer demand of equipment. Generally, those values are comprised between 3 and 5 Celsius degrees.

Condensing power demand is evaluated for each external temperature conditions over the functioning period of the system. For each hourly weather temperature value, building demand is evaluated with global insulation coefficient, GN, evaluation of it can be found in National Evaluation Methodology MC001 or Romania. This coefficient is evaluated over the building for specific type of construction by height levels and distribution by surface of its volume. The thermal losses of the building are evaluated using temperature difference of internal building design temperature and each step exterior temperature. Therefore, the compressor power required by the system to deliver power demand at heat pump condenser is synthetized by equation 7.

$$W_{comp} = \frac{GN \cdot V_{build} \cdot (t_{i0} - t_e)}{\eta_{el} \cdot f_{cd} \cdot \frac{t_{cd} + \Delta t_{cd} + 273.15}{t_{cd} - t_T + \Delta t_{cd} + \Delta t_{vp}}} = \frac{P_{cd}}{COP_{cd}} \quad (7)$$

Condensing temperature value, t_{cd} , is a question of heating equipment of the building. If direct expansion internal units are used, as very efficient thermal system, with low refrigerant values required due to an improved thermal transfer coefficient because of its forced convection, the value of condensing temperature is at its minimum. Refrigerant condensing temperature for internal heating units with forced convection can be set in interval 29-32°C.

In equation 7 now is possible to evaluate compressor electrical power at each external condition to satisfy internal comfort temperature or, as noted in this paper, design temperature, t_{i0} . For evaluation, hourly or daily average temperatures and solar radiation can be used. In this study, hourly typical meteorological year (TMY) data is used. In European area those data can be found easily and free of charge on European Commission, in EU science HUB website for photovoltaic geographical information system (PVGIS) [7]. Temperature and direct beam solar radiation are two input meteorological data used in solar collector evaluation and heat storage tank energy evaluation over the day. At each time step, heat storage tank charging power can be calculated with equation 8.

$$Q_{tank} = (a - g) \cdot \rho \cdot c \cdot (t_T - t_{out}) \quad (8)$$

The functionality of the system is assured when storage tank energy accumulation is sufficient to deliver heat pump evaporation energy required to satisfy building demand. Thus, in the calculation algorithm evaporation power is necessary. For this purpose, evaporation refrigerant state is evaluated with evaporation equivalence factor, electrical motor efficiency and compressor power given by equation (7). In equation 9,

$$Q_{evap} = \eta_{el} \cdot f_{vp} \cdot \frac{t_T - \Delta t_{vp} + 273.15}{t_{cd} - t_T + \Delta t_{cd} + \Delta t_{vp}} \cdot W_{comp} \quad (9)$$

Evaporation energy, E_{evap} , required over the day is equal with discharged storage tank energy, E_{tank} , over the day. Adding compressor energy used to recirculate refrigerant and assure its evaporation and condensing pressures, condensing energy to satisfy building demand is also easy to evaluate. Equations 10-14 are used to calculate all energies driven in the system.

$$E_{tank} = 10^{-3} \cdot \sum_{i=1}^{24} Q_{tank(i)} \cdot \Delta \tau_{(i)} \quad (10)$$

$$E_{evap} = 10^{-3} \cdot \sum_{i=1}^{24} Q_{evap(i)} \cdot \Delta \tau_{(i)} \quad (11)$$

$$E_{el} = 10^{-3} \cdot \sum_{i=1}^{24} W_{comp(i)} \cdot \Delta \tau_{(i)} \quad (12)$$

$$E_{build} = 10^{-3} \cdot \sum_{i=1}^{24} GN \cdot V_{build} \cdot (t_{i0} - t_{e(i)}) \cdot \Delta \tau_{(i)} \quad (13)$$

$$E_{cd} = 10^{-3} \cdot \sum_{i=1}^{24} COP_{cd(i)} \cdot W_{comp(i)} \cdot \Delta \tau_{(i)} \quad (14)$$

To satisfy functionality condition of the system, design temperature, t_T , should be evaluated. For this scope an iterative algorithm is lunched. Starting point of calculation is done by given a randomly initial design temperature and condition to increase or decrease it being the comparison of both evaporation and heat accumulated in the tank. The algorithm diagram is presented in chart of figure 3. Stop of the iteration is given by selecting desired error, e_{rr} , this error being the accuracy between storage tank energy and evaporator energy.

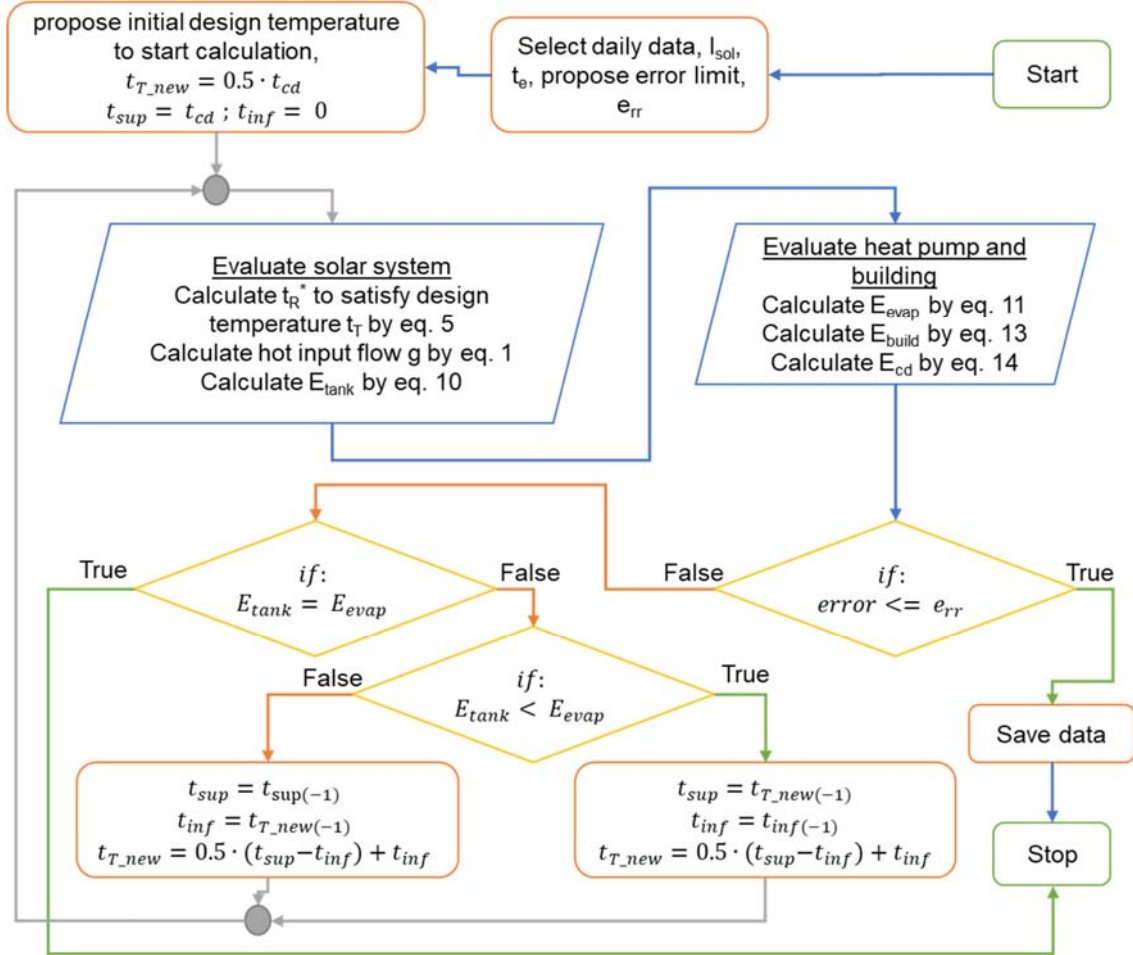


Fig 3

Algorithm state chart follows the programming tools logic, when a variable is updated by an equation using its old value, noted in the chart with index (-1). Thus, in the evaluation of the new design temperature, t_{T_new} , is updated by the average value in the middle interval of last used temperature and actual value. Depending on difference between tank energy and evaporation energy, the required design temperature should be greater comparing with old value if tank energy is less than evaporation demand and vice-versa when stored energy is higher. This state is true because once design temperature increases, for same weather conditions, storage tank energy decrease. In same time, evaporation power is increased, caused by a thermal agent with higher thermal potential.

The algorithm will return by calculation the proper design temperature to reach the maximum COP of the system when in the storage tank is stored sufficient energy for evaporation of refrigerant. Building demand clearly should be satisfied by condensing power, thus being assured the functionality of system at required external

conditions. By addition to this, algorithm can be used to evaluate the system power design of each component to respond in the worst conditions required by final customer. This methodology evaluates as worst condition the minimal equivalent temperature and not the lowest external temperature. Thus, a pre-evaluation with data mining should be done.

3. System simulation

Using MATLAB software to evaluate a proposed system, a simulation session has been released. 2 March TMY Bucharest weather data is presented in figure 4.

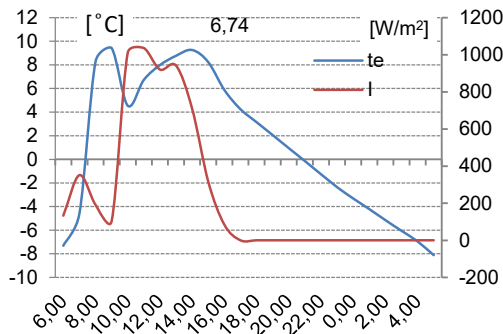


Fig 4

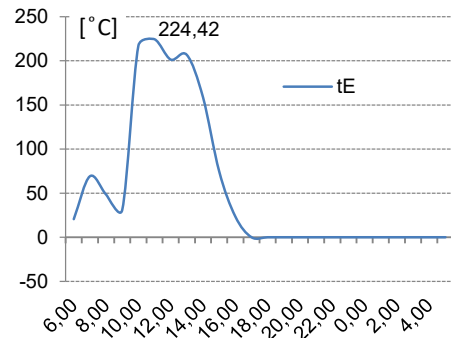


Fig 5

Associated equivalent temperature data is plotted on figure 5. This temperature is evaluated over daily hours when solar radiation is available and can be used in equation 4. As can be seen on the graph, equivalent temperature reaches high values and thermal potential of external weather being transferred to thermal agent flowing into solar system. Selected day is characterized by medium exterior temperatures and only a small interval with good solar radiation potential from 10:00am to 2:00pm, opportunity for analyzed system to deep charge of solar tank. This can be easily observed on figure 7, at which thermal agent flow with design temperature potential, transfer heat from collectors to tank.

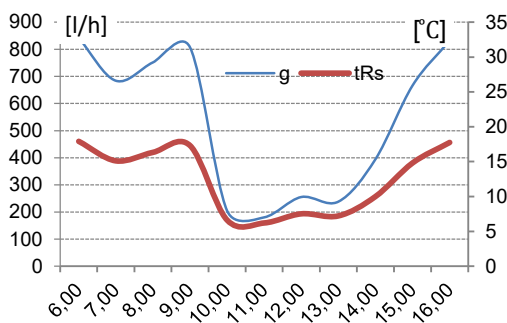


Fig 6

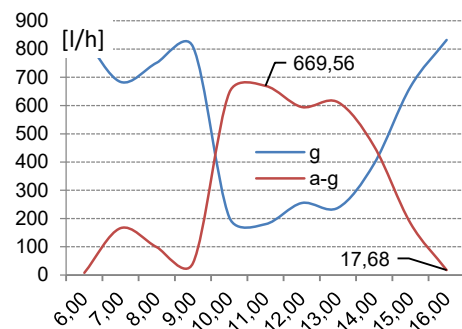


Fig 7

With a minimum 17.68 liters per hour, the system is capable to deliver energy at required design temperature in the worst external weather conditions. Figure 4 flow rate is evaluated for the proper heat tank energy, equal to evaporation demand based on state-chart of calculation algorithm in figure 3. In same time, the flow in mixing valve high potential line input increase, to deliver required temperature to obtain a thermal agent at solar collector output at the required design temperature based on procedure of this paper.

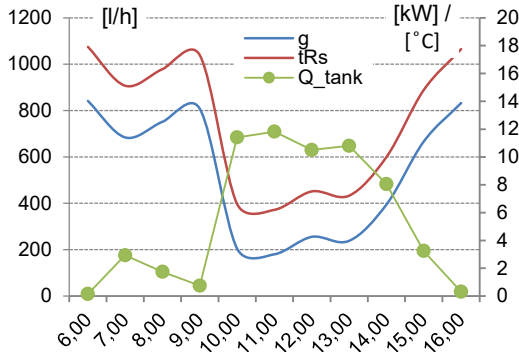


Fig 8

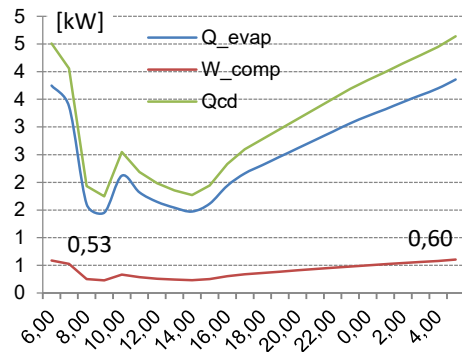


Fig 9

Return temperature, from equation 5 is proportional with equivalent temperature and external weather condition. Based on its value, dependency with flow of mixing valve high temperature input can be observed on graph of figure 8. As can be seen, its minimum value requires less flow from the output plug of solar collector. Based on this behavior, once the system function in good external weather, the solar loop discharged tank power is at its maximum. For the higher external conditions, plotted in figure 9, at 09:00am and 3:00pm, energy demand of the building is at its minimum, causing a less energy consumption of compressor electrical motor and evaporation. Renewable energy of this system can be associated to evaporation energy after extraction of electrical energy and all auxiliaries. Based on this paper equations, associated energies are plotted on figure 10, in kWh for the entire day of 2 March.

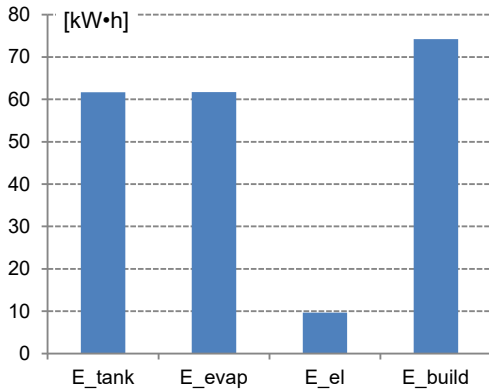


Fig 10

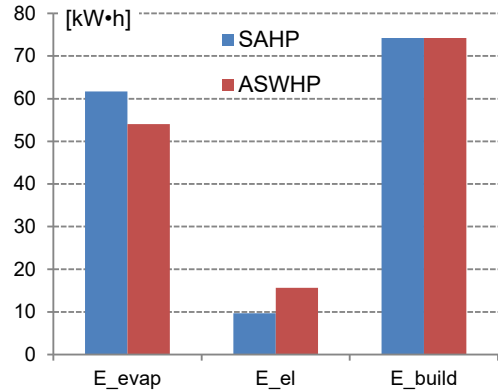


Fig 11

For the design temperature evaluated by algorithm from state-chart in figure 3 and by comparison with an air source heat pump, the advantages of solar assisted heat pump, plotted in red columns can be observed on figure 11. For the same building demand, SAHP deliver more evaporation energy for less electrical energy consumption.

Convergence of algorithm is done fast based on capability of Matlab calculation. Thus, after 10 steps design temperature is 18.1°C with an associated error less than 8.5Wh between evaporation and tank storage energy. The system analyzed is composed by 17 m² solar area, 300 m³ building with 0.55 W/m³/K global insulation coefficient, and compressor power of heat pump plotted in figure 9 with its maximum at 0.6kW.

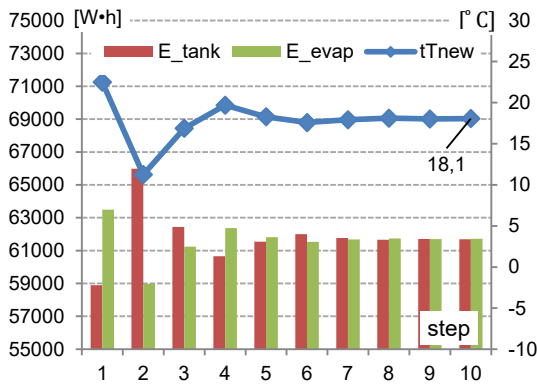


Fig 12

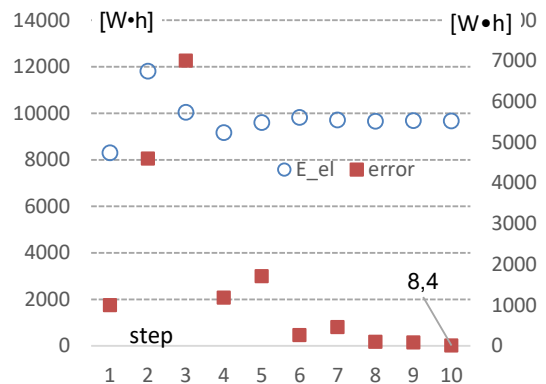


Fig 13

Electrical power of heat pump compressor corresponds to 2 March external conditions, for higher energy demand, causing higher compressor electrical power. Energies plotted in figure 2 reveal capacity of the proposed system to deliver more tank energy as can be seen in step2 for example but at this condition, evaporation

Optimizarea termodinamica a unui sistem hibrid inovativ care utilizeaza captatoare solare si pompa de caldura pentru date climatice zilnice

temperature of tank volume is not at required level, causing a gap between required and delivered energy. This will affect the overall building thermal comfort.

The system designed as describe in this paper is capable to deliver energy demand using a series connection of solar assisted heat-pump. In case design temperature or output of solar collector is not at the required value, heat pump cannot deliver required energy and an auxiliary source being necessary.

Nomenclature:

t_{out} – thermal energy storage tank bottom output temperature, °C;

t_R^* – solar collector input temperature, °C;

t_T – solar collector output design temperature, °C;

t_{T_old} – last temperature used for evaluation, °C;

t_{T_new} – new temperature used for evaluation, °C;

t_{cd} – condensing temperature, °C;

t_{vp} – evaporator temperature, °C;

t_{i0} – design internal temperature, °C;

t_e – external temperature, °C;

t_E – equivalent temperature, °C;

I_{sol} – solar radiation, W/m²;

S – solar collector equivalent surface, m²;

k_C – thermal loss global coefficient, W/m²K;

k_{Σ} – thermal transfer coefficient of inside tank coil, unitary in this paper due to open loop, W/m²K;

a – solar collector flow rate, m³/s;

ρ – thermal agent density, kg/m³;

c – thermal agent specific heat, J/kgK;

α – solar radiation absorption coefficient of collector surface, -;

τ – transparency coefficient of solar collector cover glass, -;

$\Delta\tau_{(i)}$ – step time, h;

F' – equivalence solar surface coefficient, - ;

E – solar collector thermal module, - ;

V_{build} – building volume, m³;

GN – global insulation coefficient, W/m³K;

NTU_C – numarul de unitati de transfer termic aferent suprafetei de captare solara, -;

NTU_S – numărul de unitati de transfer termic aferent schimbatorului de caldura al buclei solare, -;

Q_{cd} – condensing power, W,

Q_{evap} – evaporation power, W,

Q_{tank} – heat storage tank charging power, W,

f_{cd} – condensing equivalence factor, -,

f_{vp} – evaporation equivalence factor, -,

η_{el} – compressor engine electrical efficiency, -,

W_{comp} – compressor electrical power consumption, W,

E_{tank} – solar storage tank energy, kWh ;

E_{evap} – evaporation energy, kWh ;

E_{el} – electrical energy, kWh ;

E_{cd} – condensing energy, kWh ;

E_{build} – building demand energy, kWh ;

Δt_{vp} – evaporator temperature difference, °C,

Δt_{cd} – condenser temperature difference, °C,

SAHP – Solar Assisted Heat Pump,

ASHP – Air Source to Heat Pump,

WSHP – Water Source Heat Pump.

References:

M.F. Talpiga, A. Draghici, F. Iordache, “Heat Storage tank functional simulation using neural network,” 2021, 4rd Conference of the UTCB Doctoral School.

M.F. Talpiga, E. Mandric, F. Iordache, “Numerical simulation and parameters optimisation of heat pump model equation,” 2nd Conference of the UTCB Doctoral School, 2019.

SR 4839/1997 – Instalatii de incalzire – Numarul anual de grade zile;

Metodologie de calcul al performantei energetice a cladirilor - Mc001/2006;

Energetica echipamentelor si sistemelor termice din instalatii – Florin Iordache - Editura Conspreess, Bucuresti, 2010;

Echiptamente si sisteme termice. Metode de evaluare energetica si functionala – Florin Iordache – editura Matrixrom, Bucuresti 2017, (pag 99-113 - Sistem sursa cu captatoare solare si pompa de cal,dura – Florin Iordache, Mugurel Talpiga);

Modelare functionala si energetica a unui sistem compus din pompa de caldura, instalatie de incalzire centrala si cladire – Revista Romana de Inginerie Civila – editura Matrixrom 2018 (in curs de publicare);

Optimizarea termodinamica a unui sistem hibrid inovativ care utilizeaza captatoare solare si pompa de caldura pentru date climatice zilnice
Solar Engineering of Thermal Processes – John A. Duffie, William A. Beckman – John Wiley & Sons, Inc.2006;

F. Iordache, M. Talpiga, “Functional and energetic modeling of a system consisting of a heat pump, a central heating installation and a building,” Romanian Journal of Civil Engineering Bucharest, vol. 9, pp. 370–381.

M.F. Talpiga, F. Iordache, “Air Source Heat Pump Performance Evaluation Based on Experimental measurements and Neural Network,” 7th International Conference on Energy and Agricultural Engineering (EE&AE), Proceedings paper IEEE.

[JRC Photovoltaic Geographical Information System \(PVGIS\) - European Commission \(europa.eu\)](http://www.europa.eu)

Microsilica and steel dust as nano- and micro-particles addition for increasing the mechanical strength of fly ash and blast furnace slag-geopolymer concrete

Microsilica și praf de oțel ca adaos de nano și microparticule pentru creșterea rezistenței mecanice a betonului geopolimeric pe bază de cenușă zburătoare și zgură de furnal

Bogdan-Valentin PĂUNESCU¹, Lucian PĂUNESCU²,

Enikő VOLCEANOV^{3,4}

¹ Consitrans SA

56 Polona street, sector 1, Bucharest 010504, Romania

E-mail: pnschogdan@yahoo.com

² Cosfel Actual SRL

95-97 Calea Grivitei street, M4 room, sector 1, Bucharest 010705, Romania

E-mail: lucianpaunescu16@gmail.com

³ University „Politehnica” of Bucharest

312 Independence Splai, sector 6, Bucharest 060042, Romania

E-mail: evolceanov@yahoo.com

⁴ Metallurgical Research Institute SA

39 Mehadia street, sector 6, Bucharest 060543, Romania

E-mail: evolceanov@yahoo.com

DOI: 10.37789/rjce.2023.14.2.6

Abstract. *The paper is a contribution to developing the manufacturing technique of fly ash and blast furnace slag-geopolymer concrete with compressive strength increased up to 73 MPa and flexural strength reaching 12.1 MPa (after 180 days of curing) by adding low amounts of nanosilica (20-50 nm) and steel dust (1-5 μm) captured from electric arc furnace exhaust gases. The originality of the work consists in combining the concrete production technique by using alumino-silicate industrial by-products (ash and slag) with the addition of nano or micro-particles in order to significantly increase the mechanical strength of geopolymer concrete.*

Key words: geopolymer concrete, fly ash, blast furnace slag, steel dust, mechanical strength.

Rezumat. *Lucrarea constituie o contribuție la dezvoltarea tehnicii fabricării unui beton geopolimeric pe bază de cenușă zburătoare și zgură de furnal cu rezistență la compresiune crescută până la 73 MPa și rezistența la încovoiere atingând 12,1 MPa*

(după 180 zile de întărire) prin adaosul unor mici cantități de nanosilica (20-50 nm) și praf de oțel (1-5 μm) captat din gazele evacuate din cuptorul electric cu arc. Originalitatea lucrării constă în combinarea tehnicii producerii betonului prin utilizarea produselor secundare industriale aluminosilicatice (cenușă și zgură) cu adaosul unor nano sau microparticule în scopul creșterii semnificative a rezistenței mecanice a betonului geopolimeric.

Cuvinte cheie: beton geopolimeric, cenușă zburătoare, zgură de furnal, nanosilica, praf de oțel, rezistență mecanică.

1. Introduction

As a result of the serious ecological problems faced by the planet in the last decades, environmentally friendly technologies have become appropriate solutions that need to be implemented in economic activities. The construction materials industry is one of the most affected production activities, the usual concrete binder (i.e. Portland cement) largely contributing to the global emission of greenhouse gases (mainly carbon dioxide CO₂). The cement industry is responsible for about 10 % of the global CO₂ emissions. In 2021, the CO₂ emission in the world was 2.9 billion tons representing 0.93 kg CO₂/kg concrete. In addition, the industrial manufacture of cement is characterized by very high consumption of fossil fuel, in the current conditions of the world energy crisis [1, 2]. Under these conditions, geopolymer concrete is an excellent alternative building material for the cement [3], according to the invention of French researcher J. Davidovits [4].

Geopolymer is based on alumino-silicate natural materials (metakaolin, kaolin, rice husk ash, volcanic rock powder, etc.) or representing industrial by-products (coal fly ash, granulated blast furnace slag, red mud, mining tailing, etc.). These materials are dissolved in alkaline activating aqueous solution that facilitates the geopolymerization reaction forming molecular chains with the role of binder [3].

Several manufacturing techniques of geopolymer concrete were tested according to the literature in the first two decades of the new millennium. The best-known method of making the geopolymer is that of using coal fly ash as the basic raw material, sodium hydroxide (NaOH) solution with a concentration between 8M-16M together with sodium silicate (Na₂ SiO₃) solution as an alkaline activator. The mixture of these components leads to the formation of a gel, which is poured into a metal tray, covered with thin plastic film, and placed in an oven for curing treatment at a relatively low temperature (60-90 °C) followed by curing at room temperature. The determination of geopolymer concrete characteristics is carried out after 7, 28 or even 90 days. The results showed the increase of the mechanical strength of the concrete as follows: compressive strength by 1.5 times, split tensile strength by 1.45 times, and flexural strength by 1.6 times [3].

According to [5], geopolymer concrete made with fly ash and blast furnace slag had higher strength compared to geopolymer made with fly ash due to higher bulk

density ($2055\text{-}2100\text{ kg}\cdot\text{m}^{-3}$) and lower apparent porosity (about 17 %) and water absorption (about 7 vol. %).

Natural fibers in the form of pineapple leaf fibers soaked in NaOH solution and cut to lengths between 10-30 mm were used for increasing the mechanical strength of geopolymer concrete composed of fly ash (27.5 %), fine aggregate (55 %), NaOH 14-16M (5.7 %), Na_2SiO_3 (11.4 %), and pineapple fibers (between 0.25-0.5 %). Under the conditions of using the NaOH concentration of 16M and the maximum proportion of natural fibers (0.5 %) with the length of 30 mm, the highest values of compressive strength (41.5 MPa) and flexural strength (9.2 MPa) were reached after the curing process of 28 days [6].

In another paper [7], the mechanical characteristics (compressive strength and flexural strength) of fly ash-geopolymer reinforced with short natural fibers such as: cotton, sisal, raffia, and coconut are analyzed. The experimental results indicated that the appropriate addition of natural fibers in low proportions improves the mechanical properties of these geopolymer composites, reaching 39 MPa for compressive strength, and 8 MPa for flexural strength.

Very high performances of the mechanical strength of geopolymer concrete have been achieved by using steel fibers and microsilica [8]. The solid raw materials with very low average grain sizes were fly ash ($38\text{ }\mu\text{m}$), blast furnace slag ($17\text{ }\mu\text{m}$) and microsilica ($0.18\text{ }\mu\text{m}$), to which silica sand ($900\text{ kg}\cdot\text{m}^{-3}$) was added. After mixing these materials, the alkaline activator composed of NaOH dissolved in water, and aqueous solution of Na_2SiO_3 (including 28 % SiO_2 , 6 % Na_2O , and 64 % water) was added as well as the steel fibers (length 15 mm). Mixing these components generated slurry, that was poured into a mold. The curing process was carried out in the steam curing room at $85\text{ }^\circ\text{C}$ for 24 hours. Next, 28 days of curing process at room temperature were used before determining the product characteristics. Depending on the weight proportion of steel fibers between 1-3 %, compressive strength had values between 110-156 MPa, the highest value corresponding to the 3 % proportion, and the elasticity modulus increased from 28 to 32 GPa.

Some nanoparticles (nanosilica, nanotitania, nanoalumina, nanoclay, etc.) added to the material mixture favour the improvement of the structural properties of geopolymers. According to the literature [9, 10], their durability and mechanical characteristics are significantly increased.

The preparation of fly ash-geopolymer concrete quite frequently uses nanosilica leading to a maximum compressive strength of 51.8 MPa for the addition of 2 % nanosilica [11]. Also, in the case of manufacturing fly ash/slag-geopolymer concrete, the partial replacement of slag with nanosilica allowed obtaining a compressive strength of 54 MPa for the addition of 2 % nanosilica [12]. Testing under the conditions of increasing its proportion above 2 % showed a decrease of compressive strength value [13]. The use of nanoalumina in the manufacturing process of fly ash-geopolymer allows intensifying the geopolymerization reaction and has important effects on the mechanical properties of geopolymer [14]. Also, nanotitania added in proportion of 1-5 % contributes to the increase of compressive strength [15]. The

investigation of the influence of SiO_2 , TiO_2 , and Fe_2O_3 nanoparticles on the properties of fly ash blended cement mortars was carried out by [16]. Workability was influenced in a limited way by low proportions of nanoparticles (1-5 % of cement). Also, in low quantities, these nanoparticles contributed to increasing the compressive strength and tensile strength, instead higher proportions negatively influenced the mechanical strength.

A new construction material similar to concrete, but even stronger, was proposed in a doctoral thesis [17]. The manufacture of this material (called Ferrock) is based on 95 % recycled residual materials: steel dust captured in the gas filtration installations released from steelmaking furnaces in steel industry [18] as well as silica from recycled ground glass waste. The product is more strength (five times) than the traditional concrete, but it can erode over time in contact with salt water or with chemicals used to treat water in sewer pipes.

Considering the tested techniques and the performances obtained in the manufacturing process of high-strength geopolymer concrete presented above, the solution adopted by the authors is based on the use of granulated blast furnace slag and coal fly ash as geopolymer type raw materials and the addition of low amounts of nanosilica and steel dust as nano- and micro-particles. The alkaline activation method of geopolymers is the one commonly used including NaOH dissolved in water and Na_2SiO_3 aqueous solution, which favours the development of the geopolymerization reaction forming geopolymer concretes.

2. Methods and materials

The geopolymerization process that is the basis of the transformation of alumino-silicate materials into geopolymeric concrete involves a rapid chemical reaction in a highly alkaline environment of Si and Al rich-materials, which leads to the formation of a three-dimensional polymer chain and ring structure including Si-O-Al-O bonds [2]. According to [19], the geopolymerization is a particularly complex process, which develop in three stages, that can intersect and influence each other. Deep knowledge of the process mechanism is still difficult and its understanding requires additional research.

The preparation of geopolymer concrete is carried out in the following way. The alumino-silicate materials with the role of concrete binder (slag and fly ash) in ground state are mixed in a container together with fine aggregate (quartz sand) and coarse aggregate (gravel) for 5 min. The preparation of the alkaline activator takes place in a separate vessel, mixing NaOH and Na_2SiO_3 in water by stirring for 5 min. The liquid mixture is then poured over the solid materials and also nano-particles of silica and micro-particles of steel dust are added and the mixing of all components is carried out for another 5 min until a gel is formed. The gel is poured into a metal mold protected with a thin plastic film and placed in a thermally insulated room for the curing treatment by blowing steam at 85 °C for 24 hours. The hot curing process is followed by room temperature curing for 48 hours. Next, the geopolymer concrete is

kept for free curing removed from the mold before making the measurements to determine the characteristics of specimens at 28, 90, and 180 days.

The following materials were used in the experiment of this work: coal fly ash, granulated blast furnace, river sand, gravel, NaOH, Na₂SiO₃, nanosilica, and EAF steel dust. The chemical composition of materials mentioned above is presented in Table 1.

Table 1

Chemical composition of materials (wt. %)

Composition	Coal fly ash	Blast furnace slag	River sand	Gravel	Nanosilica	EAF steel dust [20]
SiO ₂	45.18	37.4	98.8	87.50	99.8	
Al ₂ O ₃	33.59	6.4	0.77	6.10	-	1.1
CaO	9.36	39.9		0.28	-	6.0
MgO	0.83	3.5	0.01	0.03	-	2.5
Fe ₂ O ₃	4.54	6.9	0.05	1.62	-	-
K ₂ O	1.13	0.2		-	-	-
Na ₂ O	1.07	0.1	0.22	2.08	-	-
SO ₃	0.74	-	-	0.06	-	-
TiO ₂	1.26	-	-	-	-	-
MnO	0.11	2.3	-	-	-	-
Fe ₃ O ₄	-	-	-	-	-	34.4
ZnO	-	-	-	-	-	15.0
PbO	-	-	-	-	-	2.3
Mn ₂ O ₃	-	-	-	-	-	3.2
Cr ₂ O ₃	-	-	-	-	-	0.3
LOI	1.72	-	-	-	0.2	-

Coal fly ash was provided 5 years ago by the Paroseni (Romania) thermal power plant. The material as an industrial by-product of the energy industry had a grain size below 200 μm and was processed by grinding in a ball mill and sieved to sizes below 25 μm.

Granulated blast furnace slag was provided about 7 years ago by ArcelorMittal Galati (Romania). This material with the grain size below 3 mm was also subjected to grinding in the ball mill, its granulation being reduced below 36 μm.

River sand was commercially purchased having the grain size below 2 mm, while gravel provided by a Romanian building company had dimensions between 4-8 mm.

Nanosilica (99.8 % SiO₂) IOTA HL 4200 type with the granulation in the range of 50-200 nm was commercially purchased. EAF steel dust with grain size within the limits of 1-5 μm was provided by ArcelorMittal Galati.

In general, the methods for investigating the characteristics of geopolymer concrete samples were those commonly used. The density was measured as the ratio between the sample mass obtained by weighing with an electronic balance and the volume with a regular shape that is easy to calculate [21]. Using the ASTM C642-97 standard, the apparent porosity was determined by dividing the difference between wet weight and dry weight by the difference between wet weight and suspended weight of

the sample [5]. Thermal conductivity was measured at room temperature using the heat-flow-meter HFM448 Lambda (SR EN 1946-3:2004). The 100 kN-compression fixture Wyoming Test Fixture [22] was used to determine the compressive strength. The flexural strength determination method was based on SR EN ISO 1412:2000 [23]. Immersion of the sample under water for 24 hours (ASTM D570) allowed the measurement of water absorption. The microstructural aspect of the specimens could be identified using the Biological Microscope MT5000 model with captured image, 1000 x magnification.

3. Results and discussion

Four experimental variants were adopted, in which the main variable parameters were nanosilica and EAF steel dust. Component values of mixtures are presented in Table 2.

Table 2

Composition of experimental variants

Composition ($\text{kg}\cdot\text{m}^{-3}$)	Variant			
	1	2	3	4
Blast furnace slag	300	300	290	290
Fly ash	170	170	175	175
River sand	650	650	650	650
Gravel	600	600	600	600
NaOH 8M	120	120	120	120
Na_2SiO_3	250	250	250	250
Water	60	60	60	60
Nanosilica	3.8	4.7	5.6	6.5
EAF steel dust	3.5	4.3	5.2	6.0

According to the data in Table 2, the ratio of the two alumino-silicate components (slag and fly ash) had values between 1.66-1.76, the ratio between the components of the alkaline activator (Na_2SiO_3 and NaOH) was 2.08, and the ratio between the solid and liquid components of the mixture was around 4.02. Nanosilica was used in a weight ratio between 0.8-1.4 % of the amount of alumino-silicate binder (blast furnace slag and fly ash), while EAF steel dust represented between 0.7-1.3 % of the same amount of binder.

The manufacturing recipes corresponding to the four experimental variants together with the curing process mentioned above in this paper led to the production of very dense and high hardness geopolymers concrete specimens. Appearance images of experimentally making concrete specimens are shown in Fig. 1.

Microsilica and steel dust as nano- and micro-particles addition for increasing the mechanical strength of fly ash and blast furnace slag-geopolymer concrete

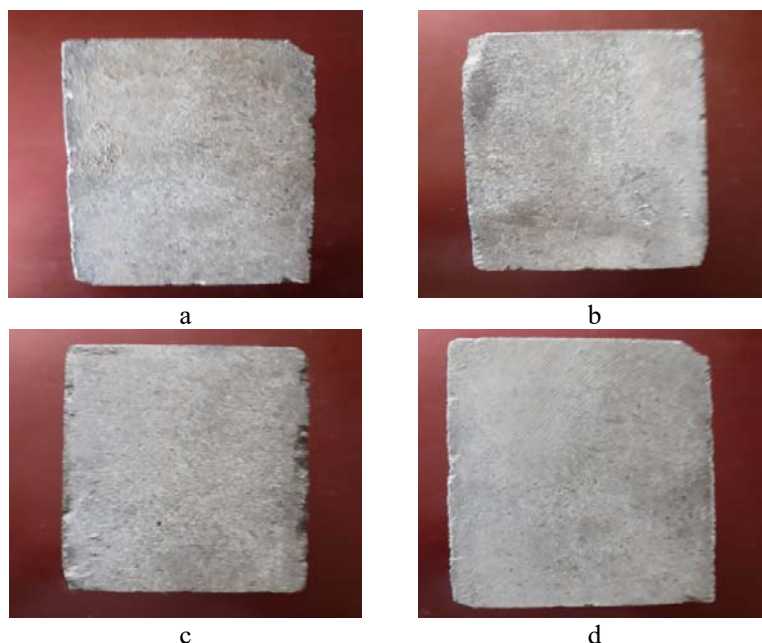


Fig. 1. Appearance images of geopolymer concrete specimens
a – variant 1; b – variant 2; c – variant 3; d – variant 4.

To identify the physical, mechanical, thermal, and microstructural characteristics, geopolymer concrete specimens were tested by the mentioned methods, results being centrally presented in Table 3.

Table 3

Characteristics of geopolymer concrete specimens

Characteristic	Variant			
	1	2	3	4
Density ($\text{kg}\cdot\text{m}^{-3}$)	2054	2070	2086	2102
Apparent porosity (%)	19.9	20.1	20.4	20.6
Thermal conductivity ($\text{W}\cdot\text{m}^{-1}\cdot\text{K}^{-1}$)	0.415	0.423	0.428	0.435
Compressive strength (MPa)	42.5	50.1	61.2	73.0
Flexural strength (MPa)	8.9	9.5	10.8	12.1
Water absorption (vol. %)	10.8	11.0	11.2	11.5

Data in Table 3 show the significance influence of addition of nano and micro-particles representing by nanosilica and EAF steel dust on mechanical properties of geopolymer concrete as well as on its thermal insulation properties (density, thermal conductivity, and apparent porosity). Compressive strength after 180 days of curing reached high values (42.5-73.0 MPa) increasing with the increase of nanosilica and steel dust proportions. Also, flexural strength registered the same increasing evolution (8.9-12.1 MPa). The density of material as well as the thermal conductivity had high values of over $2000 \text{ kg}\cdot\text{m}^{-3}$ and respectively, over $0.41 \text{ W}\cdot\text{m}^{-1}\cdot\text{K}^{-1}$, suggesting a dense

material with very few pores. By default, the concrete porosity was low, around 20 %. Water absorption was within normal limits by comparison with other geopolymer concretes made and presented in the literature.

Microstructural appearance of geopolymer concrete specimens is shown in Fig. 2.

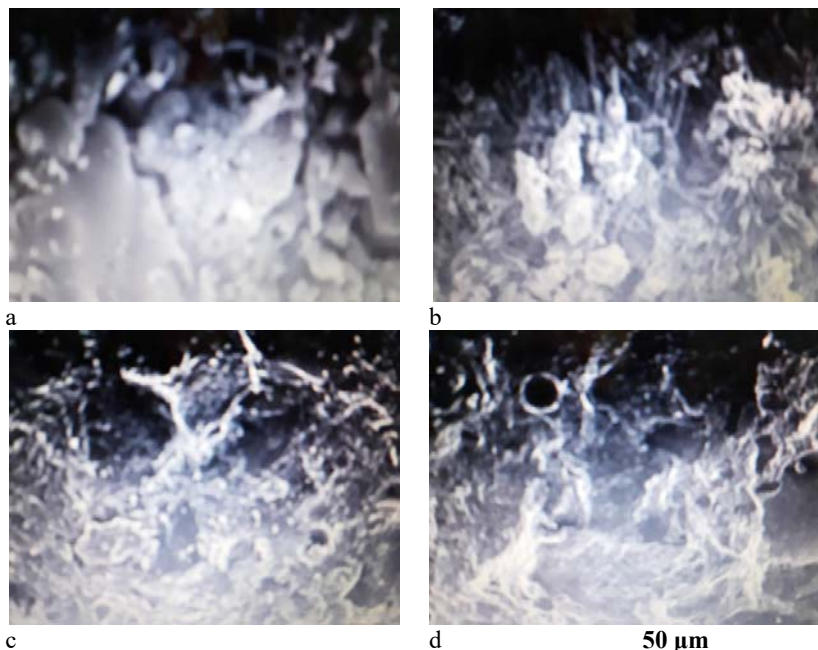


Fig. 2. Microstructural appearance of geopolymer concrete specimens
a – variant 1; b – variant 2; c – variant 3; d – variant 4.

According to Fig. 3, the compactness degree of geopolymer concrete specimens is quite high and it is accentuated towards position (d) corresponding to variant 4. This explains the high mechanical strength of samples and their very low thermal insulation properties.

The experimental results confirmed that residual alumino-silicate materials can completely replace cement in the manufacture of geopolymer concrete and the addition of nanoparticles significantly contributes to increasing its mechanical strength.

4. Conclusions

Adopting the same modern trend of protecting the planet's ozone layer against the emission of greenhouse gases (CO_2), the objective of the work was to manufacture a high-strength geopolymer concrete using fly ash and blast furnace slag, i.e. industrial by-products completely replacing cement as well as nanosilica and EAF steel dust in order to increase the mechanical strength of concrete up to 73 MPa for the compressive strength and 12.1 MPa for the flexural strength. The combined use of alumino-silicate waste and nano and micro-particles represents the originality of this paper.

References

- [1] L. N. Assi, M. Al-Bazoon, K. Carter, R. Anny, „Geopolymer Concrete Can Be the Solution for Sustainable Infrastructure”, Proceedings of the Conference The 13th Annual Inter-University Symposium on Infrastructure Management (AISIM), Indiana-Purdue University, Indianapolis, Indiana, the United States, 2017.
- [2] V. C. Nguyen, D. T. Bui, V. T., „Recent Research Geopolymer Concrete”, The 3rd ACF International Conference-ACF/VCA, vol. **A.8**, pp. 235-241, Ho Chi Minh City, Vietnam, November 11-13, 2008.
- [3] M. I. Abdul Aleem, P. D. Arumairaj, „Geopolymer Concrete-A Review”, International Journal of Engineering Sciences & Emerging Technologies, vol. **1**, no. 2, 2021, pp. 118-122, ISSN 2231-6604.
- [4] J. Davidovits, „Geopolymers: Inorganic Polymeric New Materials”, Journal of Thermal Analysis and Calorimetry, vol. **37**, no. 8, 1991, pp. 1633-1656.
- [5] H. T. Ng, C. Y. Heah, A. Mold Mustafa Al Bakri, Y. S. Ng, B. Ridho B, „Study of Fly Ash Geopolymer and Fly Ash/Slag Geopolymer in Term of Physical and Mechanical Properties”, European Journal of Materials Science and Engineering, vol. **5**, no. 4, 2020, pp. 187-198.
- [6] Zulfiati R., Saloma I., Idris Y., „Mechanical Properties of Fly Ash-Based Geopolymer with Natural Fiber”, Symposium of Emerging Nuclear Technology and Engineering Novelty, SENTEN 2018, IOP Publishing, IOP Conf. Series: Journal of Physics: Conf. Series, vol. **1198**, 2019. <https://doi.org/10.1088/1742-6596/1198/8/082021>
- [7] Korniejenko K., Frączek E., Pytlak E., Adamski M., „Mechanical Properties of Geopolymer Composites Reinforced with Natural Fibers”, Procedia Engineering, vol. **151**, Elsevier Publishing, 2016, pp. 388-398. <https://doi.org/10.1016/j.proeng.2016.07.395>
- [8] Abu Aishes Y.I., Atrushi D.S., Akeed M.H., Qaidi S., Tayeh B.A., „Influence of Steel Fibers and Microsilica on the Mechanical Properties of Ultra-High-Performance Geopolymer Concrete (UHP-GPC)”, Case Studies in Construction Materials, vol. **17**, Elsevier Publishing, 2022. <https://doi.org/10.1016/j.cscm.2022.e01245>
- [9] M. Nawaz, A. Heitor, M. Sivakumar, „Geopolymers in Construction-Recent Developments”, Construction and Building Materials, vol. **260**, Elsevier Publishing, 2020. <https://doi.org/10.1016/j.conbuildmat.2020.120472>
- [10] B. B. Jindal, R. Sharma, „The Effect of Nanomaterials on Properties of Geopolymers Derived from Industrial by-Products: A State-of-the-Art Review”, Construction and Building Materials, vol. **252**, Elsevier Publishing, 2020. <https://doi.org/10.1016/j.conbuildmat.2020.119028>
- [11] T. Phoo-ngernkham, P. Chindaprasirt, V. Sata, S. Hanjitsuwan, S. Hatanaka, „The Effect of Adding Nano-SiO₂ and Nano-Al₂O₃ on Properties of High Calcium Fly Ash Geopolymer Cured at Ambient Temperature”, Materials & Design, vol. **55**, Elsevier Publishing, 2014, pp. 58-65. <https://doi.org/10.1016/j.matdes.2013.09.049>
- [12] X. Gao, Q. L. Yu, H. J. H. Brouwers, „Characterization of Alkali Activated Slag–Fly Ash Blends Containing Nano-Silica”, Construction and Building Materials, vol. **98**, Elsevier Publishing, 2015, pp. 397-406. <https://doi.org/10.1016/j.conbuildmat.2015.08.086>
- [13] J. Wang, P. Du, Z. Zhou, D. Xu, N. Xie, X. Cheng, „Effect of Nano-Silica on Hydration, Microstructure of Alkali-Activated Slag”, Construction and Building Materials, vol. **220**, Elsevier Publishing, 2019, pp. 110-118. <https://doi.org/10.1016/j.conbuildmat.2019.05.158>
- [14] T. Alomayri, „Experimental Study on the Microstructural and Mechanical Properties of Geopolymer Paste with Nano Material (Al₂O₃)”, Journal of Building Engineering, vol. **25**, Elsevier Publishing, 2019. <https://doi.org/10.1016/j.jobbe.2019.100788>
- [15] P. Duan, C. Yan, W. Luo, W. Zhou, „Effect of Adding Nano-TiO₂ on Compressive Strength, Drying Shrinkage, Carbonation and Microstructure of Fluidized Bed Fly Ash Based Geopolymer Paste”, Construction and Building Materials, vol. **106**, Elsevier Publishing, 2020, pp. 115-125. <https://doi.org/10.1016/j.conbuildmat.2015.12.095>

- [16] D. S. Ng, S. C. Paul, V. Anggraini, S. Y. Kong, T. S. Qureshi, C. R. Rodriguez, Q. Liu, B. Šavija, „Influence of SiO₂, TiO₂, and Fe₂O₃ Nanoparticles on the Properties of Fly Ash Blended Cement Mortars”, *Construction and Building Materials*, vol. **258**, Elsevier Publishing, 2020. <https://doi.org/10.1016/j.conbuildmat.2020.119627>
- [17] W. Sun, „Kinetics of Iron Carbonate and Iron Sulfide Scale Formation in CO₂/H₂S Corrosion”, PhD Thesis, Ohio University, Athens, Ohio, the United States, 2009.
- [18] C. Lanzerstorfer, „Properties of Steelmaking Dusts from Dry Dust Separators”, *Proceedings of the 27th International Conference on Metallurgy and Materials-Metal 2018*, Brno, Czech Republic, May 23-15, 2018, pp. 41-48, ISBN 978-80-87294-84-0.
- [19] J. L. Provis, C. A. Rees, „Geopolymer Synthesis Kinetics”, in: *Geopolymers-Structures, Processing, Properties and Industrial Applications*, Woodhead Publishing Series in: Civil and Structural Engineering, J. L. Provis, J. S. J. Van Deventer (eds.), pp. 118-136, 2009.
- [20] Laura M. Simonyan, A. A. Alpatova, N. V. Demidova, „The EAF Dust Chemical and Phase Composition Research Techniques”, *Journal of Materials Research and Technology*, vol. **8**, no. 2, Elsevier Publishing, 2019, pp. 1601-1607. <https://doi.org/10.1016/j.jmrt.2018.11.005>
- [21] *** „Metrology in Laboratory-Measurement of Mass and Derived Values”, in: *Radwag Balances and Scales*, 2nd edition, Radom, Poland, 2015, pp. 72-73.
- [22] *** „A Practical Guide to Compression Testing of Composites”, R-TECH MATERIALS, Port Talbot, UK, September 2018. <https://www.r-techmaterials.com/new-and-blog/practical-guide-compression-testing-composites>
- [23] I. Curtu, A. E. Stanciu, „Determinarea Caracteristicilor Mecanice ale Epruvetelor Realizate din Material Compozit de Tip Mat&Roving”, *Buletinul AGIR*, no. 1, Ianuarie-Martie, 2011, pp. 76-81.

Aesthetics and Visualization of Building Projects in BIM Environment

Estetica și vizualizarea proiectelor de construcții în mediul BIM

Marian-Valentin POPESCU¹, Mădălina STOIAN², Andreea GRECU³

^{1,2,3} Technical University of Civil Engineering of Bucharest

124, LaculTei Blvd., 020396 Bucharest, Romania

E-mail: marian-valentin.popescu@utcb.ro, madalina.stoian@utcb.ro, andreea.grecu@utcb.ro

DOI: 10.37789/rjce.2023.14.2.7

Abstract. *In this paper we aim to analyse a current issue such as “Building Information Modelling” or modelling information in construction from a project manager's point of view. BIM is a digital tool for creating and using coordinated information in a single construction project. Generally, this model is defined as a 3D model from which the information required for each design or execution phase is extracted. 4D dimension refers to time-related information, 5D to cost information, 6D to sustainability, 7D to facility management, 8D to safety during design and building, 9D to “Lean” building concept and 10D to construction industrialization. The authors suggest the transformation of BIM 9D from Building Lean into BIM 9D project “aesthetics and visualization”.*#

Keywords: BIM, 9D BIM, rendering, project management, building industrialization, aesthetics, visualization.

1. Introduction

Building information Modelling (BIM) is a virtual model-based work environment that simulates the physical and functional aspects of a building and contains information about the characteristics of each building component. BIM is a collaborative process because the model is built by various stakeholders in the design and building phases (architects or designers, engineers, economists, constructors), encompassing as an information exchange resource and a reliable source for making decisions about a building, throughout its life cycle, see [1].

However, there are various computer applications called “BIM” that allow different actors to create, interact, extract information or manage the building from a virtual model. Some examples are ArchiCAD and Revit for architectural and

engineering design, Tekla for structural details, Vico for budgeting and building management, Solibri for the Virtual Model's analysis and consultation and ArchiFM for facility management, see [1]. Furthermore, there are many others in the market.

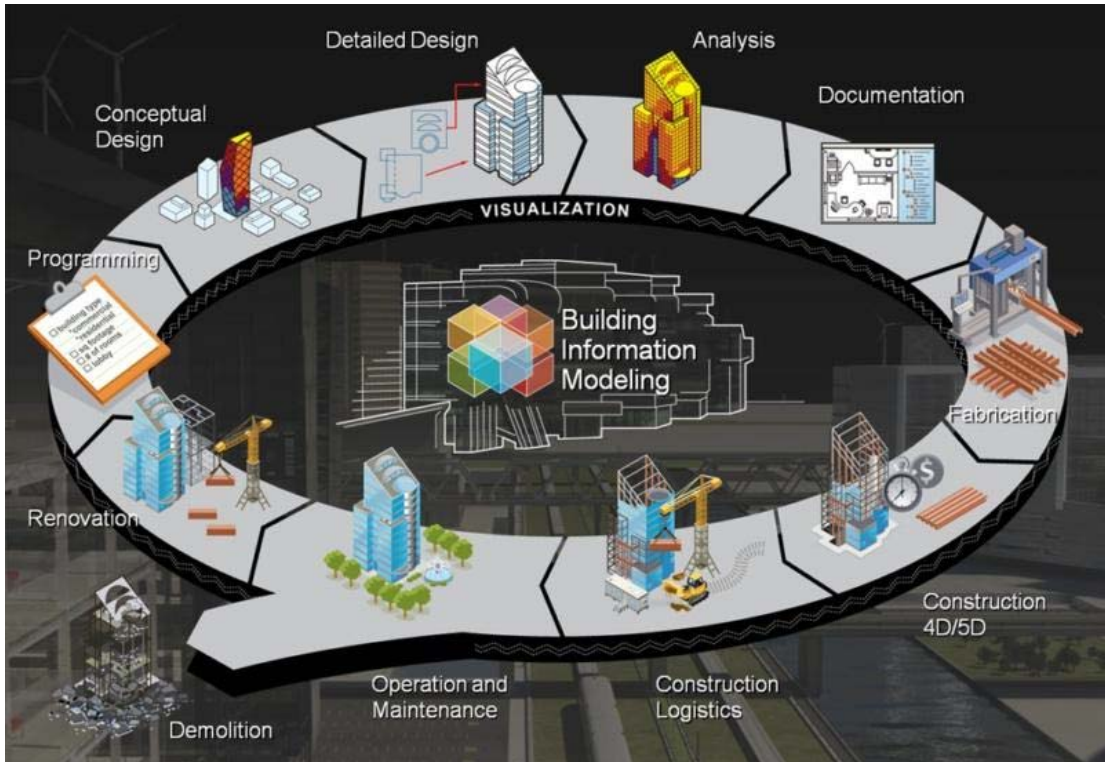


Fig. 1. Implementation of the BIM concept (source: Connectabim, www.connectabim.com/about-bim/)

It is paramount how manufacturers can participate in the development of BIM platforms. BIM methodology assumes that the virtual model is as close to reality as possible. As is the case in industry, the role of producers is essential, as only with their products the construction can be executed. The BIM model also requires the use of materials and equipment in digital format. Manufacturers should provide digital versions of their products in BIM content format or be prepared to intervene in developing the virtual model within the BIM collaboration process.

In the absence of products in BIM format, designers tend to use generic products in their projects to which they associate only minimal information. More information will subsequently be added with the product information that is currently in use. Product availability in BIM format allows specification selection and detailing in the early stages of design. There is a higher probability of product on site effective application when it is inserted and specified in a BIM model.

CAD is a technology that was born in the early '80s. Later, in the '90s, it was used globally as a tool to support project design. Although it is still used for design

support since the beginning of the century, CAD has been replaced by powerful BIM tools that manage all information about the project, including the design.

As for libraries, in addition to improving geometry, BIM objects contain among others product information data on branding, reference, finish available. They are often interactive and allow users to select different options and better understand the product operation. CAD libraries contain only product geometry, usually with too much details and in files that are not suitable for design use. Also, CAD files often support BIM libraries production, which is another manner to monetize a previous investment.

A notable example illustrating this cycle is the United Kingdom. In 2012, a law was imposed and, in 2016, the whole industry should have been linked to design, construction and adaptation in order to use BIM methodologies for public works.

In the US, BIM has been a requirement of the Department of Defence for many years. In the Nordic countries, BIM is not only the most common working methodology, but also most of these countries already have national BIM standards.

Also, in eastern countries like China, Japan, and Singapore, BIM is a technology that has been around for a long time. In the past few years, global construction has become more and more complex. BIM is the technology that supports this new capability, and manufacturers of building products should be a part of it.

Building Information Modelling (BIM) enhances the way projects are carried out and managed worldwide. It provides a revolutionary platform for the conception, construction, maintenance and operation of our built environment. In addition, BIM also changes the way we make improvements (rehabilitation, modernization and redevelopment) to existing assets in the built environment, see [8].

We have now reached an interesting stage in the evolution of BIM, where a significant number of stakeholders in the construction sector are either using BIM or considering using it. This development is particularly relevant in mature markets, although the level of adoption of BIM varies by country, the size and complexity of projects, and the size and nature of each specific organization. The managers of BIM are recognized in this context and are a very important element in the approach of a construction project.

This paper aims to address this balance by emphasizing the relevance of BIM to project management as a discipline and vice versa, the importance of integrated project management in BIM for the effective execution of projects in the built environment. It describes BIM based on a project leader's vision of the world by defining project management processes that operate in a BIM-compatible environment and by highlighting future trends in project management practice that could result from the adoption of emerging technologies in the built environment sector, see [9] and [11].

2. Description of the roots of the topic approached

2.1. BIM Dimensions

The concept of BIM is still quite new in the construction industry in Romania and therefore the implementation requires large investments in education and technology. BIM is evolving very quickly and we are glad to see that its standards are also translated into Romanian. In the course of this paper, in 2023, 7 BIM dimensions were recognised. One can extract 2D BIM, that is, one can say that BIM begins in 3D, and 2D BIM does not exist. 2D is a flat dimension, in particular plans and 2D sections. CAD computer-aided design began in the 1960s, and the concept of BIM appeared in 1957, and the first software developed for the public by Graphisoft in 1987-ARchiCad, was introduced in 1970. It is the first software to make 2D drawings and 3D geometry. Officially, according to Biblus, Autodesk, see [2], United-BIM are recognized as 7 BIM (7D) sizes, but they can go even further because it is an ever-changing concept, see [7]. In addition to the aforementioned 7 dimensions, there is now an open debate about three "new dimensions of BIM".



Fig. 2. BIM from 3D to 10D (source: Biblus, <https://biblus.accasoftware.com/en/wp-content/uploads/sites/2/2018/04/dimensions-of-BIM-2.jpg>)

Below we list the BIM dimensions from 3D to 10D that we will detail in the following chapters, see [3] and [4]:

- 3D - 3D modelling, graphic information;
- 4D - 4D information, time-related, construction sequencing by Gantt charts and timeline;

- 5D - 5D cost analysis, cost management, construction cost estimation etc.;
- 6D-Sustainability 6D, Environmental, Economic and Social Sustainability Impact Studies;
- 7D - Life cycle and maintenance 7D, Facility Management: planning and managing maintenance operations throughout the building life cycle;
- 8D - safety during design and construction;
- 9D - Construction optimization in the implementation phase is the 9th dimension of BIM;
- 10D -The 10th dimension of BIM refers to the industrialization of construction.

In the following, we will focus on describing dimensions 8D, 9D and 10D and the proposal to improve dimension 9D.

2.2. Description of BIM 8D - Safety during design and execution

Safety during execution can be anticipated from the design phase. This is very important, because 8D BIM is the dimension of BIM that supports you in managing safety on construction sites and it helps you prevent risks and hazards to workers from the design period.

8D BIM is the BIM dimension that adds safety information to the geometric design of the construction during the design and execution phases. In practice, it is possible to model the site with all its elements (fencing, storage spaces, scaffolding, machinery, indicators, etc.) and visualize it realistically, thanks to advanced technologies such as virtual reality and augmented reality. It is possible to accurately render the site through virtual reality glasses. To achieve these results, one needs specific software that is equipped with special libraries with dedicated objects and simulates any type of machine and construction equipment so that one can produce the most suitable models.

The aim is to have an overview of the site already in the design phase to prevent possible risks and hazards for workers. Viewing the site in advance and in a realistic manner allows an easier and more efficient analysis of all possible scenarios and prevents hazards and critical situations at every stage of the project.

The main advantages of site safety management are:

- having a full picture of the possible scenarios to work on the site;
- drawing up detailed safety plans to date;
- accurately identify and analyse the most appropriate choices for execution safety;

- preventing risks by interfering with design choices that may generate potential hazards;
- viewing the digital site in 3D;
- training workers through virtual reality;
- reducing the risk of accidents.

2.3. Description of BIM 9D - “Lean” construction

9D BIM, also known as lean construction, is the BIM size that optimizes and streamlines all steps involved in implementing a project by digitizing processes.

Lack of planning on a site can lead to delays in project delivery and, consequently, to an increase in the initial budget. 9D BIM is the method designed to completely eliminate losses, optimize all resources involved in the construction process and increase productivity.

Undoubtedly, all these aspects contribute to the achievement of a valuable final product.

The principles on which the lean construction is based are:

- optimize, reduce or eliminate activities that do not add value to the process-In order to achieve process improvement, particular attention is paid to all aspects of the supply chain (from production, to the transport of materials to the site). The entire production chain is analysed, unnecessary or repetitive processes are identified and strategies are developed to simplify or replace them. For example, the use of means of transport is planned to be optimized and perfectly adapted to the quantities to be transported. With this in mind, it is preferable to use larger trucks for transporting materials, reducing the number of transports required;
- taking into account the needs of the customer -Before starting any project, it is necessary to identify the needs of the client through market research and satisfaction surveys, even in the case of projects that have already been delivered. Activities that do not add value to the process are not of interest to the customer and therefore he is not willing to pay for them. On the other hand, focusing on customer needs is more likely to make all operations work smoothly;
- process standardization - Construction is one of the sectors with the highest rate of unforeseen events: each project is unique and unique are also the conditions that come into play on the site (completion time, workmanship, local conditions, availability of equipment and materials, etc.). In order to minimize site diversification, standardized construction processes should be adopted,

reducing the possibility of problems and improving the ability to manage unforeseen events. Reducing these variables allows the construction company to maintain a predefined standard and ensure a smoother and safer process;

- time optimisation -The time variable is influenced by transport activities, waiting, processing, inspection, etc. The optimization of all these activities has an impact on the quality of the work and the delivery times of the customers;
- Increased transparency -This principle contributes to a greater participation of all those involved in the process, who can actively and more consciously intervene in the development of solutions for improvement.

The way in which the construction process is managed differs between traditional and lean construction methods. In the lean method, the activities are divided into:

- activities that add value to the project;
- activities that do not add value to the project.

The concept of value is directly related to the degree of customer satisfaction, therefore, if the customer is not willing to pay for a particular activity, it is categorized as an activity that does not add value to the final product. According to this criterion, lean thinking aims to eliminate as many losses as possible already from the project management phase. In the traditional method, however, the activities are divided into sub-processes, and the criterion is not the degree of customer satisfaction. There is no careful management of losses and no planning of activities in the preliminary phase.

2.4. Description of BIM 10D - construction industrialization

10D BIM aims to industrialize and make the construction sector more productive thanks to the integration of new technologies and real-time information. It is possible to achieve 10D BIM by using tools for the digitization of civil constructions such as the BIM management system, which makes it possible to align all those involved in the construction life cycle and optimize each stage. The advantages of 10D BIM for the project manager are:

- reducing the construction time of the building envelopes;
- optimization of site costs;
- improving and implementing work safety measures;
- increased construction quality thanks to state-of-the-art digital infrastructure;
- precise control at each stage of production of each individual element through advanced, codified and standardized processes;
- no dependence on weather conditions that may affect the activities of the site.

All dimensions of BIM have as common objective the 10th dimension, which aims to develop the construction sector and increase productivity, thanks to new technologies and process digitalization. 10D BIM is the key to solving the problem of low productivity in the construction industry and to optimize every phase of the building life cycle: The design, construction and management of infrastructure or equipment. In this regard, 10D BIM works as a tool that centralizes data to optimize all project activities based on the use of technology. This means that project managers will have the resources to carry out the project in the best possible way. 10D BIM has the promise to provide a complete vision for asset management (during the design, construction and maintenance phases). It can therefore be used to align the financial, commercial, environmental, health and safety, risk analysis, etc. sectors. In this context, the 10D BIM tool offers countless possibilities for all types of projects and it can be used at all stages with the support of highly intelligent digital technologies and resources that automate even the most complex tasks.

3. Case Study

In the following we will present a case study of a modern housing with the following characteristics:

- Height regime - semi-basement and ground floor,
- House location - Bistrița, Bistrița-Năsăud county,
- Designer - **Construct**,
- Beneficiary - private investment,
- Budget for the investment - 200.000 \$,
- Location - difficult terrain on slope.

The idea of the project started from the integration of floating volumes giving the sensation of levitation. The composition consists of three volumes: a single prismatic volume at the semi-basement level that is very well integrated in the slope of the ground, a second volume which represents the exit in the cantilever principle, giving a feeling of levitation, and the third volume is the living room as vertical dominance of composition. Through this study we will analyse the information of the building model and how time and cost control are affected throughout the project. Following the theoretical documentation, we will analyse the project on the following levels, see [10]:

- 2D documentation - plans and sections extracted from the 3D model
- 3D BIM -Geometry, analysis of the 3D model
- 4D BIM -time, planning and duration of implementation
- 5D BIM -cost estimate and budget

- 6D BIM 6D -sustainability, energy efficiency

3.1. 2D Documentation

The transition from 2D CAD to 3D allows architects, civil engineers and designers to work more efficiently and accurately. However, given that 2D drawings still dominate the project's deliverables, the ability to work in both 2D and 3D is beneficial. It is very important to extract the 2D drawings from the 3D models because in our country most public institutions require printed documents filed. The final electronic format as documentation is also represented by 2D drawings in pdf format and in some cases DWG. As technology advances very quickly, it is possible that in the future the final deliverable will be a single digital 3D model.

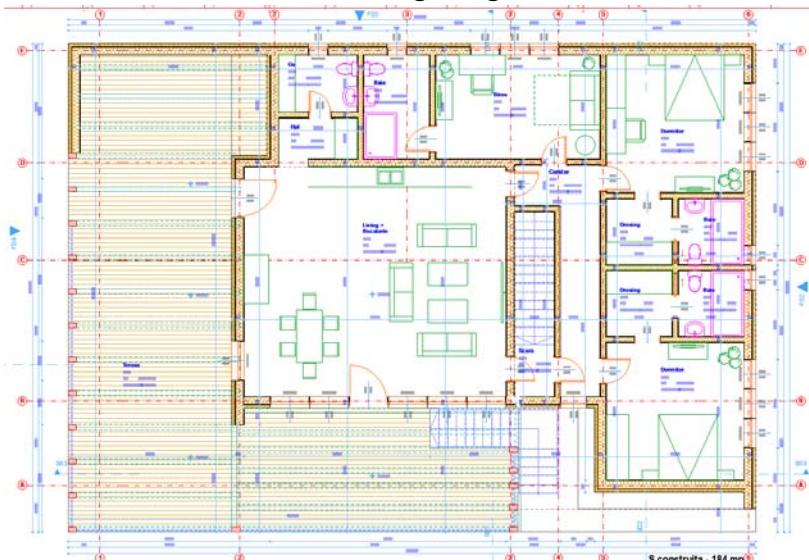


Fig. 3. Execution plan (source: Personal portfolio)

Functionally, the ground floor consists of a living room with kitchen, bathroom, 2 bedrooms with bathroom and dressing, office with private bathroom, circulation and access ladder from the basement, covered terrace. The infrastructure is a mixed one made of concrete diaphragms and reinforced concrete frames. The superstructure is made of load-bearing walls of „framing” type. The covering is a terrace with an inclination of 3% in the north-south direction.

The 2D documentation is extracted from the 3D model. Three-dimensional walls were used to make the 3D model, and the plan shows their 2D projection. Stairs, windows, doors, furniture are made of 3D objects. In the plan we see their representation on the 2 dimensions.

3.2. 3D BIM

3D BIM, as it is well known, represents the three geographical dimensions (x, y, z) of a building's structure. Geographic capabilities help stakeholders to visualize the structure of a building in 3 dimensions just before the project starts. The BIM 3D environment allows all stakeholders to collaborate effectively in shaping and solving typical structural problems. Also, because everything is stored in a central location, which is the BIM model, it becomes easier to solve problems in the next stage. When it comes to 3D BIM, it involves creating a 3D model and sharing the same information using a common data environment (CDE).

The benefits of 3D BIM are:

- Improved 3D view of the entire project,
- Simplified communication and sharing of design expectations,
- Easy collaboration between multiple teams, regardless of their field of expertise,
- Reducing the number of changes and revisions due to total transparency from the start.



Fig. 4. Volume extracted from 3D model (source: Personal portfolio)

We present the realization of the 3D model of the individual dwelling made on a slope plot. Due to the gradient of the terrain, making the 3D model becomes more difficult to achieve. For the 3D model we used three-dimensional elements such as walls and floor coverings for exterior closures. For the construction of the structure we used poles and beams but also composite elements on the area where the structure is made of wood. GDL objects were used for windows, doors, stairs, see [5]. GDL is the abbreviation „Geometric Description Language”, a functional programming language based on „BASIC”. It was created to encourage architects to use this language to build their own geometrical objects through the possibilities of design and presentation.

In 3D field modelling, a collaboration between the topographic engineer, architects and engineers takes place. This is how the topographic engineer performs the topographic lifting in stereo coordinates 70. From these coordinates can be made a 3D model of the land.

The advantages of 3D modelling are among others:

- you can study different possibilities of housing on the ground;
- accurate measurements of the level quotas. These measurements are made against the 0.00 elevation of the construction and are very accurate to the gradient of the land.
- precise technique of „cut and fill”- cutting and filling. More precisely, we can figure out where to cut the soil and what volume we get for a better systematization of the land.

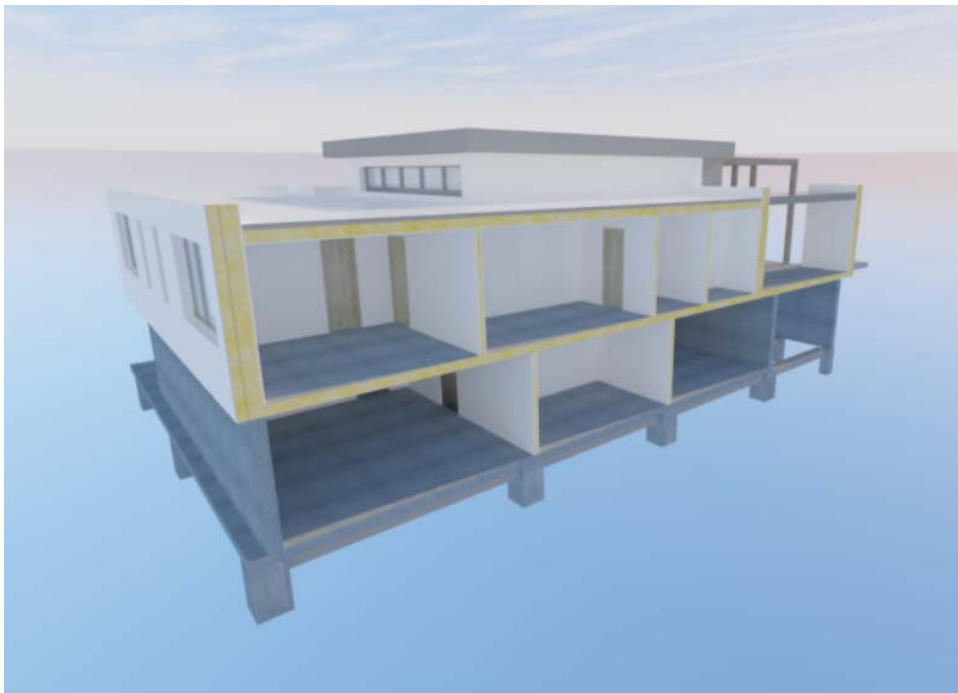


Fig. 5. Three-dimensional section through 3D model (source: Personal portfolio)

3.2. A Graphic Shortcoming of Playing in BIM

As can be seen, a shortcoming of representations in the BIM environment is that they do not address in an aesthetically friendly way the final beneficiary of the construction.



Fig. 6. Render final Model (source: Personal portfolio)

The image above is a rendering extracted from the 3D model and passed through various software to render the reality as best as possible. In general, these architectural renderings are made by architects and designers to give customers a picture as close to reality as possible with the future construction before it is executed.

We believe that a project manager must present his idea to the client in a very convincing way. Whether you present this idea in a traditional way through plans, compared to sections, you need to convince the potential customer by offering the most optimal and attractive solutions. On the architectural visualizations that we have not talked about, we would like to point out that in all construction projects it is very important aesthetics. A successful project must convince both the beneficiaries and the society that it is well integrated in the environment.



Fig. 7. Rendering of interior living (source: Personal portfolio)

In addition to the technique used by each project manager and solving the function of each construction, we also need to take care of the aesthetic side of things in order to become more convincing toward customers and friendlier to the built environment. With new technologies we advanced from 3D rendered images to the next level. Realistic photo videos play an important role in the industry and detail information for a better understanding of the project. A video shows the construction from multiple angles of view to better understand it. The construction is rendered by the materials used by light and shade, resulting in something very close to the expected final result.

Renderings are the most widespread representation techniques globally, but the latest presentation technologies are virtual reality ones. When it comes to interior design, the best way to visualize a space is through augmented reality. Through VR we can communicate the value of the project, what the specifications and features are and motivate the planning and construction costs in a much more interactive way. With VR we can use an infinity of furniture pieces and arrange them in the room to achieve the desired result.



Fig. 8. Render living from different angle (source: Personal portfolio)

All three ways of presenting a project are extracted from the 3D BIM model. The more detailed the model, the more spectacular the presentations will be. We wanted to recall the three presentation modes, traditional rendering, video presentations and virtual reality and emphasize the need to be introduced into one of the 10 dimensions of BIM or even reach the 11th dimension of BIM.#

At the beginning of this section we talked about the graphic representation of elements in constructions and along the way, the idea of integrating the presentation of a project on the aesthetic leitmotiv was formed in one of the 10 dimensions of BIM.#

Analysing the 10 BIM dimensions presented at the beginning: 3D BIM that refers to shape and geometry, 4D BIM that refers to time, 5D BIM that refers to costs, 6D BIM that refers to sustainability and 7D BIM that refers to facility management in buildings, they prove to be very well defined by the community and users.

It remains to be debated whether the other three dimensions of BIM are relevant. If we start with 8D safety during design and execution this is very important from our point of view and we have to keep it in mind from the design phase to the construction exploitation phase.

9D BIM “Lean” constructions is more of a construction management style that plans, optimizes and streamlines a project. At 4D BIM, we do the same with 9D BIM. The difference is that we are required to do this management method. BIM 9D reduces construction costs and activities that do not give value to the final deliverable, but the same can be done in the 5D BIM, which is referring to cost planning.#

BIM 10D refers to the industrialization of construction. This is a very interesting aspect and leads to evolution. We currently use vertical and horizontal elements in 3D models, pillars, beams, walls and slabs.

Through the industrialization of construction, we imagine a central library where companies add all the materials used on the market, and designers use them in projects much more efficiently. The result would be to work directly with three-dimensional digital elements to design constructions.#

We propose to do an exercise of imagination and transform BIM 9D from “Lean” construction into BIM 9D aesthetics and project visualization.

To do this we need to define very well what aesthetics means in architecture and construction. The aesthetics of a building is one of the main aspects considered in architecture.

The attraction and beauty of a building cover the combined effects of shape, size, texture, colour, balance, and proportion, space, alignment, pattern, decoration, the culture and context of a building.

From this simple definition we can see that it is absolutely necessary one of the five senses that Aristotle described about 300 years before Christ. This sense is sight, visual perception, or what we see with our eyes.

From this hypothesis was born the idea of BIM 9D to merge the aesthetic part with the visualization of a project.



Fig. 9. Final external rendering (source: Personal portfolio)

4. Conclusion

The new BIM 9D dimension-aesthetics and visualization of construction projects should include an aesthetic guide to be transformed into minimal standards. Three types of architectural visualizations should be integrated into BIM 9D: three-dimensional rendering, video presentations and virtual reality.

The advantage is that these presentations can be made with a simplistic model from the concept phase, and to achieve the most realistic results, a detailed model at LOD 300 level of detail is required, see [7]. *Through BIM 9D - aesthetics and visualization of construction projects we can also make a project marketing strategy.*

This can be very useful for developers because their project can be promoted from the design stage in the BIM environment.

Our study model, the individual home, has a level of detail between LOD 200 and LOD 300, see [7].

There was good coordination between the architectural model, the structure model, and the terrain model that has complex geometry. With a sufficiently detailed model, we were able to get some visual images close to what will be built in reality.

Project aesthetics and visualization can become a new dimension of BIM and we launch this challenge for BIM developers.#

References

- [1] ConectaBIM, About Bim - [www.http://www.connectabim.com/about-bim/](http://www.connectabim.com/about-bim/), p. 1-2
- [2] Autodesk (2013). About BIM. <http://usa.autodesk.com/building-information-modeling/about-bim>, p. 2-3
- [3] buildingSMART (2012). The BIM Evolution Continues with OPEN BIM. <http://www.buildingsmart.org/organization/OPEN%20BIM%20ExCom%20Agreed%20Description%2020120131.pdf>, p. 2-3, 34
- [4] openBIM (2012). OpenBIM - Programskrift. Stockholm.Northumbria University, Ryder (2012). Bimacademyhttp://collab.northumbria.ac.uk/bim2/?page_id=500, p. 2-3
- [5] Northumbria University, Ryder (2012). Bimacademy http://collab.northumbria.ac.uk/bim2/?page_id=500, p. 2-3
- [6] Biblus <https://biblus.accasoftware.com/en/bim-dimensions/> p. 6-25
- [7] LOD United-BIM <https://www.united-bim.com/practical-approach-to-level-of-detail/>, p. 18-25
- [8] Empower Bim Technology, <https://engbim.com/> p. 18-25
- [9] PMI, Project Management Institute (2008). A guide to the project management body of knowledge p. 26
- [10] Messner, J. (2011). Utilizarea BIM <http://www.bim.psu.edu> p. 27-34
- [11] RICS 2013, Building Information Modelling for Project Managers, p. 35-37.